The ciliary protein Spef2 stimulates acinar Ampkα/Sirt1 signaling and ameliorates acute pancreatitis and associated lung injury

Chun Zhang[#]^, Deng-Fang Guo[#], Gui-Fang Lv, Dai-Chang Zhang^, Feng Lin, Jia-Bin Liu, Jian-Yuan Lin, De-Xian Xiao

Department of General Surgery, Mindong Hospital Affiliated to Fujian Medical University, Fu'an, China

Contributions: (I) Conception and design: C Zhang, DF Guo, DC Zhang; (II) Administrative support: F Lin; (III) Prepare of study experimental materials and animals: GF Lv; (IV) Collection and assembly of data: C Zhang, JB Liu; (V) Data analysis and interpretation: JY Lin, DX Xiao; (VI) Manuscript writing: All authors; (VII) Final approval of manuscript: All authors.

[#]These authors contributed equally to this work and should be considered as co-first authors.

Correspondence to: Dai-Chang Zhang; Feng Lin. Department of General Surgery, Mindong Hospital Affiliated to Fujian Medical University, No. 89, Heshan Road, Fu'an 355000, China. Email: daichangzhang2020@163.com; 286081780@qq.com.

Background: Pancreatic acinar cells are susceptible to nuclear factor kappa B (NF-κB)-mediated inflammation and resulting cell necrosis during early acute pancreatitis. As adenosine monophosphate-activated protein kinase alpha (Ampkα)/sirtuin 1 (Sirt1) pathway activity attenuates NF-κB activity, we examined whether the Ampkα/Sirt1 axis affects the progression of acute pancreatitis and associated lung injury *in vivo*. Furthermore, we explored the role of the ciliary protein sperm flagellar 2 (Spef2, Kpl2) in regulating Ampkα/Sirt1 activity *in vitro* and *in vivo*.

Methods: Pancreatic injury, oxidative stress, acinar cell necrosis and apoptosis, acinar levels of Ampkα/Sirt1/NF-κB signaling activity, NF-kB-mediated inflammatory markers, and markers of associated lung injury were measured in rat models of acute pancreatitis following pharmacological Ampkα activation with A769662 or self-complementary recombinant adeno-associated virus serotype 6 (scAAV6)-mediated Spef2 overexpression. Additional *in vivo* rescue studies involving Ampkα silencing and/or constitutively active (CA)-Sirt1 overexpression were performed in acute pancreatitis rats. *In vitro* immunoblotting and Ampkα activity assays were conducted in the pancreatic acinar cell line AR42J.

Results: Pharmacological Ampkα activation or Spef2 overexpression reduced acute pancreatitis severity, oxidative stress, necrosis, apoptosis, NF-kB-mediated inflammatory markers, and the degree of associated lung injury. Spef2 overexpression in AR42J cells *in vitro* promoted Ampkα^{Thr172} phosphorylation and Ampkα activity. *In vivo* rescue studies revealed that Spef2's suppressive effect on acute pancreatitis and associated lung injury is mediated via the Ampkα/Sirt1 axis.

Conclusions: This study established the existence of a Spef2/Ampkα/Sirt1 axis in pancreatic acinar cells that is involved in the regulation of NF-κB-mediated acinar cell inflammation and resulting cell necrosis during acute pancreatitis.

Keywords: Acute pancreatitis; Ampkα; Sirt1; Spef2; NF-κB

Submitted May 20, 2022. Accepted for publication Jul 18, 2022.

doi: 10.21037/atm-22-3118

View this article at: https://dx.doi.org/10.21037/atm-22-3118

^ ORCID: Dai-Chang Zhang, 0000-0002-0677-2779; Chun Zhang, 0000-0001-7808-4556.

© Annals of Translational Medicine. All rights reserved.

Introduction

Acute pancreatitis is a pancreatic inflammatory disorder (1). In the US, acute pancreatitis is responsible for approximately 279,000 new patient admissions and $2.6 billion in costs annually (1,2). Acute pancreatitis can be mild or severe, with the severe form causing significant pancreatic acinar cell necrosis and intense local inflammation. If left untreated, severe acute pancreatitis can lead to further systemic complications such as inflammatory response syndrome and multiple organ dysfunction. Severe acute pancreatitis can lead to acute lung injury, which is typically caused by severe infection (3). Acute lung injury is the most common distant organ dysfunction secondary to severe acute pancreatitis with an incidence of 27.7%. Due to unhealthy lifestyle habits (e.g., chronic alcohol consumption, overeating) (3), the incidence of severe acute pancreatitis has risen dramatically in recent years, and over 50% of associated deaths occur within the first 2 weeks due to systemic complications (2,4). The current standard of care for severe acute pancreatitis is supportive care and fluid resuscitation, as there are no specific therapeutic interventions to treat this disease at present (5,6).

Previous research demonstrates that the transcription factor nuclear factor kappa B (NF-κB) plays a key role in activating a pro-inflammatory cascade that can result in acute pancreatitis progression (6,7). As the role of NF-κB-mediated inflammation during severe acute pancreatitis cases is now well-established, many believe this to be the dominating factor of disease progression (7,8). One of the first signs of multiple organ dysfunction and the leading cause of mortality in severe acute pancreatitis patients is acute respiratory distress syndrome (ARDS) (9,10). During the early phases of severe acute pancreatitis, immune cells such as neutrophils, alveolar macrophages, and lymphocytes infiltrate the lung parenchyma. As in severe acute pancreatitis, NF-κB promotes lung alveolar macrophage production of pro-inflammatory cytokines and increases the amount of lung injury (11,12). Consequently, a greater understanding of the molecular mechanisms that control NF-κB-mediated inflammation during the early phases of severe acute pancreatitis may be key in finding new therapeutic targets for the disease.

The serine/threonine kinase adenosine monophosphate-activated protein kinase alpha (AMPKα, Ampkα) is a stress sensor that becomes activated in response to conditions of low energy (13). Upon activation, Ampkα initiates catabolic pathways that result in adenosine triphosphate (ATP) generation, while simultaneously inhibiting anabolic pathways to avoid ATP consumption (13). It is well-established that Ampkα activity is negatively correlated with inflammation (14-16). Furthermore, several studies have shown that Ampkα upregulates expression of sirtuin 1 (Sirt1), which functions to negatively regulate NF-κB activity (17,18). Consequently, some researchers have attempted to target this Ampkα/Sirt1 axis in order to treat other NF-κB-mediated inflammatory diseases akin to severe acute pancreatitis (19).

With respect to severe acute pancreatitis, the phosphorylation of Ampkα has been shown to attenuate NF-κB activity in an animal model of acute pancreatitis, and the use of an Ampkα inhibitor abolishes this protective effect (20). As a result, the Ampkα/Sirt1 axis could prove to be an important pathway responsible for NF-κB-mediated acinar cell necrosis and inflammation in severe acute pancreatitis and associated lung injury. As the impact of Ampkα/Sirt1 on acinar cell necrosis and inflammation is still not clear, here we examined whether the pharmacological activation of the Ampkα/Sirt1 axis affects the progression of acute pancreatitis and associated lung injury *in vivo*. Furthermore, using acinar cell-specific self-complementary recombinant adeno-associated virus serotype 6 (scAAV6)-mediated overexpression, we explored the role of the ciliary protein sperm flagellar 2 (Spef2, Kpl2) in regulating Ampkα/Sirt1 activity *in vitro* and in acute pancreatitis and associated lung injury *in vivo*. We present the following article in accordance with the ARRIVE reporting checklist (available at https://atm.amegroups.com/article/view/10.21037/atm-22-3118/rc).

Methods

Ethical statement

Institutional approval for this study was obtained in advance from the Ethics Committee of Mindong Hospital Affiliated to Fujian Medical University (Fu'an, China; No. 20200126K). All animal experiments were conducted in accordance with the National Institutes of Health (NIH) Guide for the Care and Use of Laboratory Animals (Bethesda, MD, USA). A protocol was prepared before the study without registration.

Cell lines and cell culture

The rat pancreatic acinar cell line AR42J was obtained from

© Annals of Translational Medicine. All rights reserved.

the American Type Culture Collection (ATCC). Cells were cultured at 37 ℃ in 5% CO_2 in Dulbecco's modified Eagle's media (DMEM; Gibco) supplemented with fetal bovine serum (FBS, 10%), penicillin (100 U/mL) and streptomycin (100 mg/mL) (Invitrogen).

Adenoviral vectors and small-interfering RNAs (siRNAs)

Self-complementary recombinant adeno-associated virus serotype 6 (scAAV6) vector expressing a non-coding control cDNA sequence (scAAV6.NC), rat *Spef2* cDNA (scAAV6.Spef2), or a combination of rat *Spef2* cDNA and constitutively-active rat *Sirt1* cDNA (scAAV6.Spef2+CA-Sirt1) under the control of the pancreatic acinar cell-specific rat elastase I (elastase 3B, *Ela3b*) promoter (21) were constructed by Genepharma (Shanghai, China). Briefly, cDNA fragments were amplified with reverse transcription polymerase chain reaction. Recombinant scAAV6 vectors containing the sequences were prepared in HEK293 cells as previously described (22). The adenoviral vector titer was determined using the gradient dilution method, and the prepared adenoviral particles were stored at –80 ℃.

We employed a combination of three siRNAs against rat *Prkaa1* (Ampkα, NM_019142.2) (RiboBio Co. Ltd., China) in order to ensure efficient knockdown (siAmpkα = rat *Ampkα* siRNA.1 + rat *Ampkα* siRNA.2 + rat *Ampkα* siRNA.3). Sequences were as follows: rat *Ampkα* siRNA.1 forward 5'-UUAC AGA GGG AUU CAA AUA CUG AGG-3' and reverse 5'-CCU CAG UAU UUG AAU CCC UCU GUAA-3'; rat *Ampkα* siRNA.2 forward 5'-UGAU CAU CGA GGA AAG AAU CGG GUG-3' and reverse 5'-CAC CCG AUU CUU UCC UCG AUG AUCA-3'; rat *Ampkα* siRNA.3 forward 5'-AUAA GUA AGU CCU ACU AUC CAC UUG-3' and reverse 5'-CAA GUG GAU AGU AGG ACU UAC UUAU-3'; and negative control siRNA (siCtrl) forward 5'-UUC UCC GAA CGU GUC ACGU-3' and reverse 5'-ACG UGA CAC GUU CGG AGAA-3'.

Rat models of acute pancreatitis

Wistar rats were obtained from Beijing Vital River Laboratory Animal Technology Co., Ltd., China. All rats were male and weighted between 200–250 g. Rats were housed in large metallic cages (three per cage) under a standard natural day-light cycle at 25 ±1 ℃ and provided standard chow and water *ad libitum*.

A rat model of acute pancreatitis was established as previously described (23-27). Sample sizes of experimental cohorts were based on previously published studies using the same rat model (28,29). In brief, anesthetized rats were treated with urethane (20%; 0.5 mL/kg). After laparotomy, the hepatic duct was identified and clamped near the hilus of the livers. A retrograde infusion of sodium taurocholate (5%, 1 mL/kg; Jingmei Biotechnology, China) at a constant rate of 0.1 mL/min was performed through the anterior wall of the duodenum using a 1-mL syringe. The sham-operated control rats received an infusion with an equivalent volume of saline. After ten minutes the clamp was removed, followed by abdominal closure.

For the first series of *in vivo* experiments, rats were randomly assigned to three groups by random number generator: (I) sham-operated control as described above; (II) acute pancreatitis + vehicle (0.3 mL/kg DMSO administered intravenously 1 hour post injury); and (III) acute pancreatitis + the Ampkα agonist A769662 [10 mg/kg in 0.3 mL/kg DMSO administered intravenously 1 hour post injury (30)].

For the second series of *in vivo* experiments, rats were randomly assigned into three groups by random number generator: (I) sham-operated control as described above; (II) acute pancreatitis + scAAV6.NC; and (III) acute pancreatitis + scAAV6.Spef2. Rats were injected with scAAV6.NC or scAAV6.Spef2 (5×10^{11} viral particles/rat) via retrograde pancreatic ductal delivery three weeks prior to acute pancreatitis induction as previously described (22). The ductal delivery procedure did not affect acute pancreatitis markers or systemic inflammatory markers compared to sham-operated control (Table S1). Post-surgery, rats were placed on a heating pad to maintain body temperature and were subcutaneously injected with carprofen (10 mg/kg) to alleviate post-operative pain/discomfort.

For the third series of *in vivo* experiments, rats were randomly assigned into four groups: (I) sham-operated control as described above; (II) acute pancreatitis + scAAV6.NC + siCtrl; (III) acute pancreatitis + scAAV6.Spef2 + siCtrl; (IV) acute pancreatitis + scAAV6.Spef2 + siAmpkα; and (V) acute pancreatitis + scAAV6.Spef2 + CA-Sirt1 + siAmpkα. scAAV6 vectors were delivered as described above. For siRNA therapy, siCtrl or siAmpkα were administered by daily infusion for three days prior to the induction of acute pancreatitis.

After 24 hours following acute pancreatitis induction, rats were sacrificed. *A priori*, subjects were to be excluded if they did not survive until this humane endpoint. No subjects were excluded from this study, and there were no unexpected adverse events. Pancreatic tissue, lung tissue,

© Annals of Translational Medicine. All rights reserved.

bronchoalveolar lavage fluid (BALF), and peripheral blood samples were collected for further examination. Rat serum was isolated via centrifugation of whole blood at 3,000 ×g for 15 minutes and then stored at –80 ℃ for downstream use.

Tissue and serum measurements

The levels of lactate dehydrogenase (LDH), malondialdehyde (MDA), lipid peroxide (LPO), and myeloperoxidase (MPO) from pancreatic tissue were measured according to the manufacturer's protocol (Jiancheng Bioengineering Institute, China). C-reactive protein (CRP) levels were measured from serum as previously described using a biochemical analyser (Toshiba, Japan) (25). Serum interleukin (IL)-18, tumor necrosis factor-alpha (TNF-α), IL-6, and IL-1β levels as well as *in vitro* pancreatic acinar cell LDH secretion levels were assayed using ELISA kits (R&D Systems). Serum amylase and lipase levels were determined by starch-iodine assay and nephelometry, respectively, according to the kit instructions (Nanjing Jiancheng Bioengineering Institute).

Hematoxylin and eosin (H&E) tissue staining

Tissue damage and inflammation was calculated from H&E stated tissue sections visualized under a light microscope (40×). The scoring system used was previously reported by Kusske *et al.* (31).

Lung tissue analyses

Tissues were fixed, dehydrated, embedded, and cut into thin 4-mm sections for H&E staining and blinded microscopy examination. Lung lesions were scored in accordance to a previously reported criterion (32,33). The upper-lung lobe on the right side was collected and the wet weight was measured to evaluate lung edema. Samples were dehydrated for 48 hours in a 70 ℃ oven and then reweighed. These data were used to calculate the lung W/D ratio. Lung MPO activity assays were conducted as previously reported (34,35). Absorbance (460 nm) was measured at 25 ℃ and the ability of samples to break down H_2O_2 in the presence of O-dianisidine dihydrochloride was measured.

Bronchoalveolar lavage fluid (BALF) analyses

Frozen BALF was homogenized in preparation for ELISA assays. IL-1β and TNF-α were measured according to the manufacturer's protocol. Total protein levels were measured using Coomassie brilliant blue staining.

Establishment of in vitro models

AR42J cells were seeded in 10-cm dishes at a density of 1×10^7 cells/dish in 10 mL medium with 100 nM dexamethasone (Sigma) for 24 h to enhance the acinar phenotype (36). For *in vitro* adenoviral experiments, AR42J cells were then treated with scAAV6.NC or scAAV6.Spef2 (4×10^8 viral particles, multiplicity of infection =40). 72 hours following viral infection, overexpression efficacy was measured using qPCR and immunoblot analysis.

For *in vitro* siRNA experiments, dexamethasone-treated AR42J cells from above were plated at 50% confluence in serum-free media and transfected with siRNA (50 nM each siRNA) using Xtreme siRNA transfection reagent in accordance with the manufacturer's protocol (RiboBio, China). In control cells, an equivalent volume of PBS was added. Twelve hours following transfection, knockdown efficacy was measured using qPCR and immunoblot analysis.

72 hours following viral infection and 12 hours following siRNA transfection, AR42J cells were incubated with cerulein (Sigma-Aldrich) to establish an *in vitro* model of acute pancreatitis (23). Cell counting Kit-8 (CCK-8; Dojindo Molecular Technologies, Japan) was used to measure cell viability.

Terminal deoxynucleotidyl transferase dUTP nick end labeling (TUNEL) assay

TUNEL staining was conducted to measure cell apoptosis levels. The TUNEL detection kit was followed as per manufacturer's protocol (HRP kit DBA; Italy). In brief, tissue sections were covered with proteinase K (15 μg/mL) at room temperature for 15 minutes. A 5-minute incubation at room temperature with H_2O_2 (3%) was used to inactivate endogenous peroxidases. Next, sections were incubated with TUNEL buffer (37 ℃) for 90 minutes in a humidified atmosphere. Then, sections were incubated with horseradish peroxidase (HRP)-conjugated secondary antibodies at room temperature for 30 minutes before diamino-benzidine (DAB) was used to visualize the signal. The number of positive cells per field (400×) were counted for 10 fields per slide.

To assess different treatments, AR42J cells were plated into a 24-well plate and incubated with different treatments. The One Stem TUNEL Assay Kit (Beyotime

© Annals of Translational Medicine. All rights reserved.

Biotechnology, China) was used to calculated apoptosis as per the manufacturer's protocol. Signal intensity was measured via fluorescence microscopy.

Ampkα activity assay

Endogenous Ampkα activity in AR42J cell lysates was assayed as previously described (37). Lysate samples were diluted to a concentration of 1 mg/mL in resuspension buffer containing 50 mM Tris HCl (pH 8, 4 ℃), 1 mM EDTA, 10% glycerol (w/v), 0.02% Brij-35 (w/v), 1 mM dithiothreitol, protease, and phosphatase inhibitors (Sigma). To incorporate ^{32}P into the AMARA peptide, diluted sample (2 µL) was incubated with 200 µM AMARA peptide (AMARAASAAALARRR), 200 µM [^{32}P]ATP[γ-P], 200 µM AMP in 40 mM HEPES–NaOH buffer (pH 7.0), 80 mM NaCl, 5 mM $MgCl_2$, 0.8 mM dithiothreitol, and 8% (w/v) glycerol (to achieve a total volume of 25 µL) for 5 min at 30 ℃. At the end of 5 min, 15 µL mixture was blotted onto 1 cm^2 phosphocellulose paper, which was then washed thrice (10 min for each wash) in 150 mM phosphoric acid followed by a final 5 min wash in pure acetone. The papers were dried and counted in 4 mL scintillation fluid (EcoLite). Ampkα activity was reported as picomoles of incorporated ^{32}P per minute per mg of protein.

Immunofluorescence

Cells were plated into 24 well plates and fixed using paraformaldehyde (4%) for 30 minutes before a further 20-minute incubation with Triton X-100 (0.5%) to permeabilize cells. Next, cells were incubated for 2 hours with cleaved caspase-3 (CC-3) antibodies (Abcam) the washed three times with PBS. Secondary antibodies were added for a 1 hour incubated and DAPI was used as a cell nuclei stain. Finally, cells were visualized using a confocal microscope (Olympus).

ATP assays

ATP levels were calculated using the Enhanced ATP Assay as per the manufacturer's protocol (S0027; Beyotime Biotechnology, China). Levels are expressed as nmol/OD730 and measured against a standard curve.

Cell necrosis and apoptosis via flow cytometry

The FITC Annexin V Apoptosis Detection Kit I (BD Biosciences) was used to calculate cell necrosis and apoptosis. In brief, cells were washed with PBS and resuspended in binding buffer. Next, cells were incubated with Annexin V and PI according to the kit protocols. Finally, cells were analysed via flow cytometry (Epics Altra II, Beckman Coulter). Necrotic cells were defined as Annexin V+/PI+ (dot plot's upper-right quadrant), while apoptotic cells were defined as Annexin V+/PI– (38) (dot plot's lower-right quandrant).

Quantitative real-time reverse transcription PCR (qPCR) analysis

qPCR was used to assess mRNA expression levels in pancreatic tissues as previously reported (39). Total RNA was extracted using an RNA Extraction Kit (Invitrogen) and RNA was converted into cDNA as per the manufacturer's protocol (Toyobo, China). qPCR was conducted using SYBER Prime Script reagent and a LightCycler PCR System (Roche). The primer sequences were as follows: rat *Spef2* forward 5'-GAA GTA TTG ATG ATG AGA TTA CA-3' and reverse 5'-CGA TAG TTG CTG ATG GAT-3'; rat *Ampk*α forward 5'-ATC CGC AGA GAG ATC CAG AA-3' and reverse 5'-CGT CGA CTC TCC TTT TCG TC-3'; rat *Sirt1* forward 5'-TGA AGC TGT TCG TGG AGA TAT TTTT-3' and reverse 5'-CAT GAT GGC AAG TGG CTC AT-3'; and rat *Gapdh* forward 5'-TGG AGT CTA CTG GCG TCTT-3' and reverse 5'-TGT CAT ATT TCT CGT GGT TCA-3'. PCR cycling conditions were as follows: amplification at 95 ℃ for 30 seconds, followed by 40 cycles at 95 ℃ for 5 seconds to denature, and 60 ℃ for 20 second to anneal. Expression levels were calculated using the $2^{-\Delta\Delta CT}$ method with rat *Gapdh* as a housekeeping gene.

Western blotting analysis

Western blotting was used as previous reported (40,41). In brief, cells or tissues were homogenized and lysed in protein lysis buffer supplemented with protease inhibitors (Beyotime Biotechnology, China) and phosphatase inhibitors (Roche). Following centrifugation, the supernatant was collected. Protein lysates were then subjected to SDS-PAGE (Jiancheng Bioengineering Institute, China). Protein within the gel was transferred onto polyvinylidene difluoride membranes. Non-specific proteins were blocked using 5% milk, followed by an incubation with primary antibodies against: rat Spef2/Kpl2 (#orb157763, Biorbyt), rat Ampk alpha subunit (Ampkα; #2532, CST), rat phospho-Ampk

© Annals of Translational Medicine. All rights reserved.

alpha^{Thr172} subunit (p-Ampkα^{Thr172}; #2535, CST), rat Sirt1 (#9475, CST), rat NF-κB p65 subunit (p65; #4764, CST), rat phospho-NF-κB p65^{Ser536} subunit (p-p65^{Ser536}; #3033, CST), rat TNF-α (#ab66579, Abcam), rat IL-1β (#NB600-633, Novus Biologicals), and rat cleaved caspase-3 (CC-3; #9664, CST). Rat β-actin (#4967, CST) was used as a loading control. Next, membranes were washed and incubated with a horseradish peroxidase (HRP)-conjugated mouse anti-rabbit IgG secondary antibody (#5127, CST). Protein was detected via enhanced chemiluminescence (Pierce Chemical). Protein expression was calculated using ImageJ densitometry relative to β-actin expression.

Statistical analyses

Data represented as means ± standard deviations (SDs). GraphPad Prism 6.0 was used to perform all statistical analyses. Student's *t*-test or one-way ANOVA with a post-hoc Bonferroni test was conducted to compare means values between groups. $P<0.05$ was considered statistically significant.

Results

Enhancing Ampkα activity attenuates acute pancreatitis and associated lung injury in vivo

The morphological structure of pancreatic tissue was normal in the sham-operated control group (*Figure 1A*). The pancreatic tissue collected from rats in the acute pancreatitis group treated with a vehicle (dimethyl sulfoxide, DMSO) showed noticeable edema, hemorrhage, neutrophil infiltration, cell necrosis, and disrupted acini and lobule structures 24 hours post-treatment. However, in the acute pancreatitis rats treated with the selective Ampkα agonist A769662, there was a significant reduction in edema, hemorrhage, neutrophil infiltration, and cell necrosis when compared to the rats in the vehicle-treated acute pancreatitis group. Pathological scoring of pancreatic tissues 24 hours post-treatment matched the foregoing observations (*Figure 1B*). In comparison to those in the vehicle-treated acute pancreatitis group, the rats treated with A769662 had significantly reduced pancreatic expression levels of the stress markers lactate dehydrogenase (LDH), malondialdehyde (MDA), lipid peroxide (LPO), and myeloperoxidase (MPO; *Figure 1C*). Pancreatic ATP levels, an indicator of cell health, were significantly reduced in the vehicle-treated acute pancreatitis rats when compared to those in the sham-operated control rats (*Figure 1D*). However, the A769662-treated acute pancreatitis rats had higher levels of ATP when compared to the vehicle-treated acute pancreatitis rats. Necrosis levels were significantly increased in the vehicle-treated acute pancreatitis rats when compared to those in the sham-operated control rats (*Figure 1E*). However, the A769662-treated acute pancreatitis rats had lower levels of necrosis when compared to the vehicle-treated acute pancreatitis rats.

To measure pancreatic tissue apoptosis, a terminal deoxynucleotidyl transferase dUTP nick end labeling (TUNEL) assay was performed on pancreatic tissue samples from each group. Pancreatic apoptosis levels were significantly elevated in the vehicle-treated acute pancreatitis rats when compared to those in the sham-operated control rats. However, the A769662-treated acute pancreatitis rats had lower levels of apoptosis when compared to the vehicle-treated acute pancreatitis rats (Figure S1A,S1B). Furthermore, these differences between the groups were mirrored by the protein levels of the apoptotic mediator cleaved caspase-3 (CC-3; Figure S1C,S1D).

Analyzing Ampkα/Sirt1/NF-κB signaling activity in pancreatic tissue, we found Ampkα^{Thr172} phosphorylation, Sirt1 expression, and NF-κB p65 phosphorylation to be significantly elevated in the vehicle-treated acute pancreatitis rats compared to that in the sham-operated control rats (*Figure 1F* and Figure S2). However, these levels were reduced in the A769662-treated acute pancreatitis rats. Consistent with this, serum collected 24 hours post-treatment showed that the vehicle-treated acute pancreatitis rats had elevated levels of the pro-inflammatory cytokines CRP, TNF-α, IL-1β, IL-6, and IL-18 when compared to the sham-operated control rats. However, these levels were reduced in the A769662-treated acute pancreatitis rats (*Figure 1G*).

We next assessed the rat subjects for acute pancreatitis-associated lung injury 24 hours post-treatment. The morphological structure of the lung tissue was normal in the sham-operated control group. In the vehicle-treated acute pancreatitis rats, intense edema, severe alveolar congestions, and immune cell infiltration occurred (*Figure 1H*). In the A769662-treated acute pancreatitis group, the degree of edema and immune cell infiltration was markedly reduced. The pathological scores also demonstrated improvements in the A769662-treated acute pancreatitis group (*Figure 1I*). The lung wet-to-dry (W/D) ratio was increased in the vehicle-treated acute pancreatitis rats relative to the sham-

© Annals of Translational Medicine. All rights reserved.

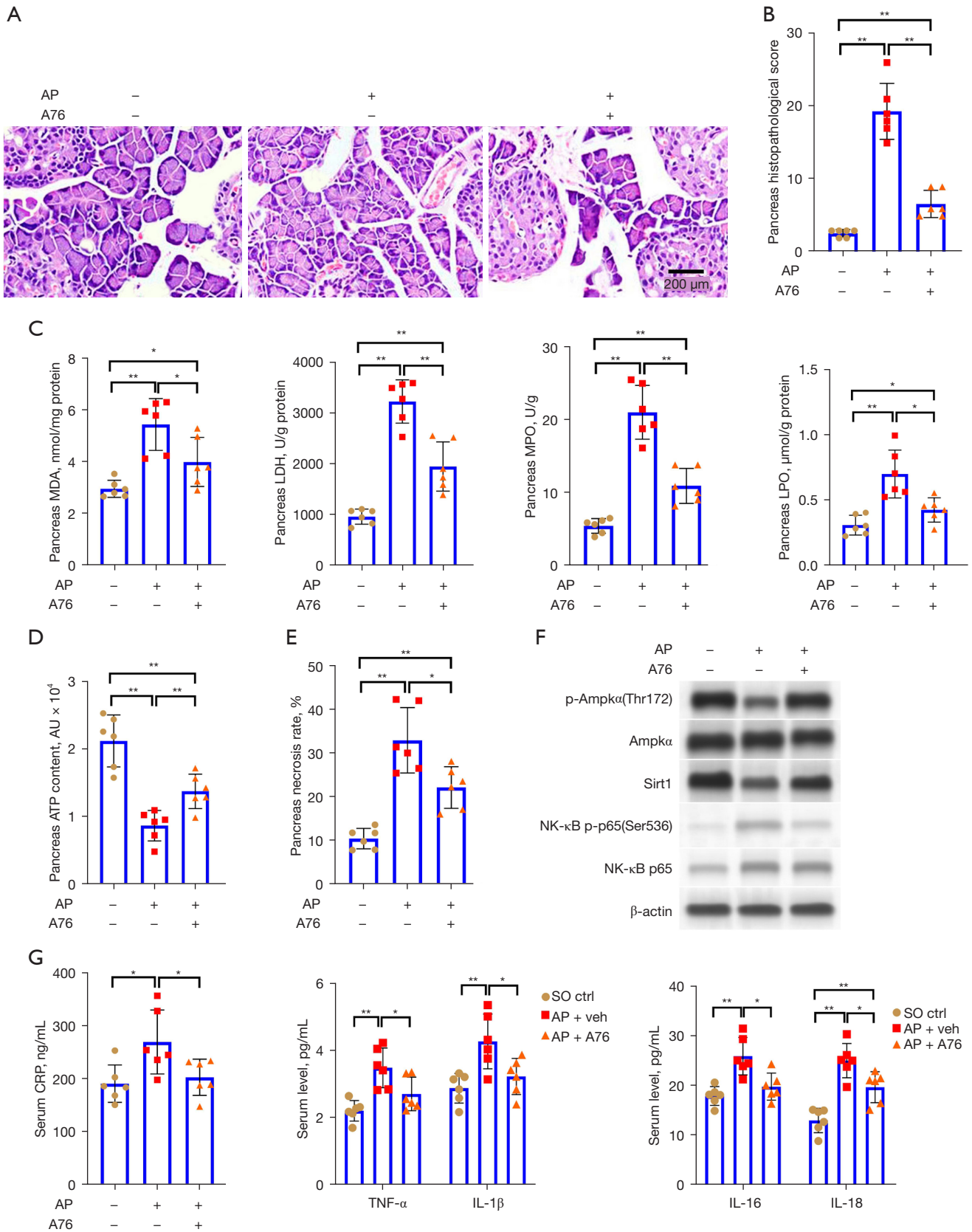

© Annals of Translational Medicine. All rights reserved.

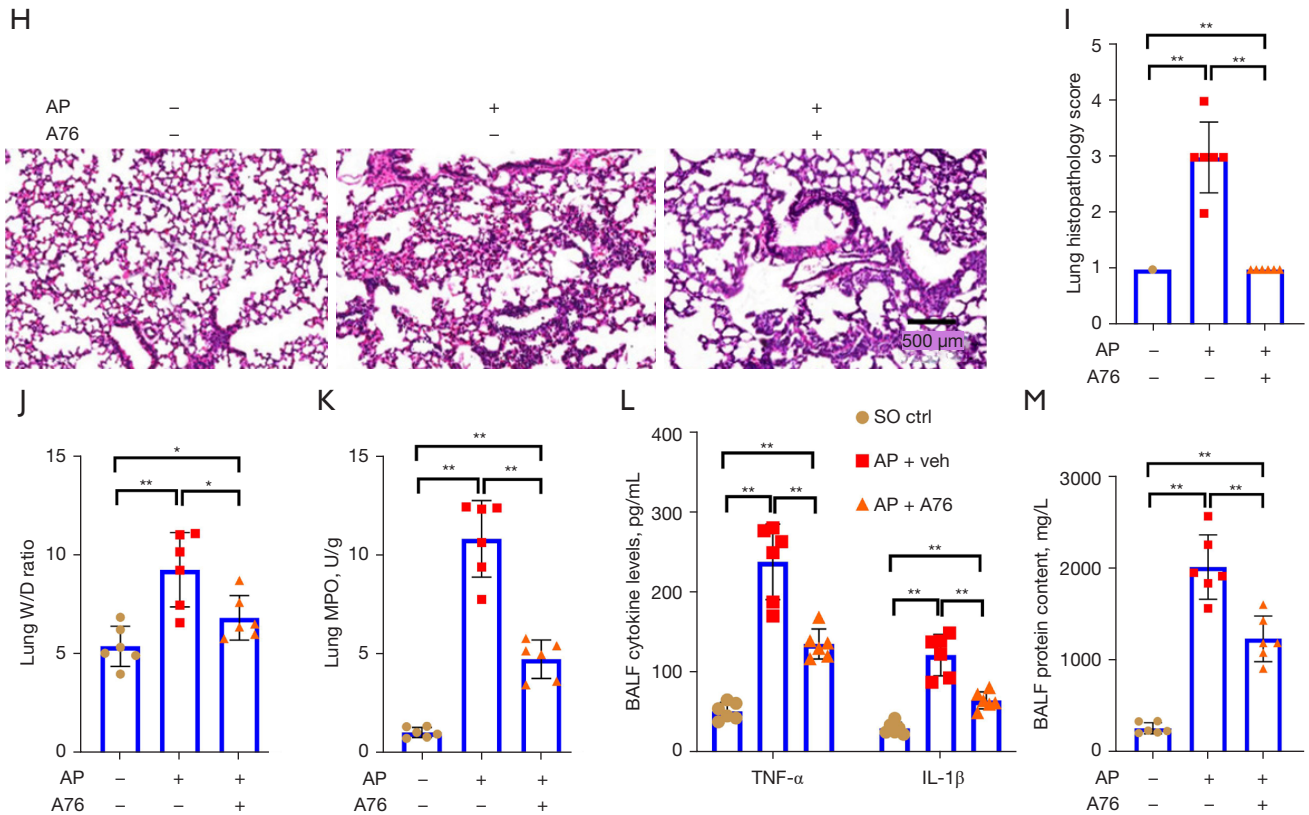

Figure 1 Enhancing Ampk**α** activity attenuates acute pancreatitis and associated lung injury *in vivo*. Pancreatic and lung tissues and peripheral blood samples were harvested from sham-operated control (SO Ctrl), acute pancreatitis + DMSO vehicle (AP + Veh), and acute pancreatitis + Ampkα agonist A769662 (AP + A76) rats 24 hours post-induction. (A) Representative H&E staining of pancreatic tissues. (B) Pathological scoring of pancreatic injury. (C) Pancreatic LDH, MDA, LPO, and MPO activity levels. (D) Pancreatic ATP levels. (E) Pancreatic necrosis levels. (F) Representative immunoblots of pancreatic Ampkα/Sirt1/NF-κB signaling proteins. (G) Serum CRP, TNF-α, IL-1β, IL-6, and IL-18 levels from peripheral blood samples. (H) H&E staining of lung tissue showing extensive edema, alveolar congestion, and immune cell infiltration (scale bar =500 μm). (I) Pathological scoring of lung tissue injury. (J) Lung W/D ratio. (K) Lung MPO activity. (L) BALF TNF-α and IL-1β levels and (M) BALF protein content. Data represented as means ± SDs. N=6 rats per cohort. *P<0.05, **P<0.01 (one-way ANOVA with Bonferroni post-hoc). DMSO, dimethyl sulfoxide; Ampkα, adenosine monophosphate-activated protein kinase alpha; H&E, hematoxylin and eosin; LDH, lactate dehydrogenase; MDA, malondialdehyde; LPO, lipid peroxide; MPO, myeloperoxidase; ATP, adenosine triphosphate; Sirt1, sirtuin 1; NF-κB, nuclear factor kappa B; CRP, C-reactive protein; TNF-α, tumor necrosis factor alpha; IL-1β, interleukin-1 beta; W/D, wet-to-dry; BALF, bronchoalveolar lavage fluid; SD, standard deviation; ANOVA, analysis of variance.

operated control rats (*Figure 1J*) and greatly reduced in the A769662-treated acute pancreatitis rats. Lung MPO activity was increased in the vehicle-treated acute pancreatitis rats (*Figure 1K*) and greatly reduced in the A769662-treated acute pancreatitis rats. Bronchoalveolar lavage fluid (BALF) TNF-α and IL-1β levels were elevated in the vehicle-treated acute pancreatitis group and greatly reduced in the A769662-treated acute pancreatitis group (*Figure 1L*). BALF protein levels were greatly elevated in the vehicle-treated acute pancreatitis group (*Figure 1M*) and greatly reduced in the A769662-treated acute pancreatitis group. Collectively, these data demonstrate that Ampkα activation offers a protective role in acute pancreatitis and associated lung injury *in vivo*.

Overexpression of Spef2 promotes Ampkα activity in pancreatic acinar cells in vitro

Most eukaryotic cells possess a microtubular protrusion called a primary cilium that regulates intracellular signaling

© Annals of Translational Medicine. All rights reserved.

effectors associated with cell growth and proliferation, including AMPK and liver kinase B1 (LKB1) (42). *In silico* analysis of previously-published gene microarray data derived from wild-type (WT) mice over a 5-day period following cerulein-induced acute pancreatitis [GEO: GSE40895 (43)] revealed that the ciliary protein Spef2 is the most significantly downregulated gene in acute pancreatitis (Figure S3A). We also confirmed pancreatic Spef2 downregulation in gene microarray data from a shorter-term (10-hour) murine model of cerulein-induced acute pancreatitis [GEO: GSE109227 (44)]. Notably, our Search Tool for the Retrieval of Interacting Genes (STRING) analysis of the Spef2 protein revealed that Spef2 interacts with adenosine kinase (Adk; Figure S3B). Adk is a conserved phosphotransferase that converts adenosine into AMP, which stimulates Ampkα activity (45,46) by phosphorylation at its T172 residue. Also, previous research indicates that the Spef2 protein itself contains an adenylate kinase (AK) domain (47), which catalyzes the interconversion of adenine nucleotides [2 adenosine diphosphate (ADP) ↔ AMP + ATP] and maintains AMP-Ampkα signaling (48).

Based on this evidence, we hypothesized that enhancing Spef2 expression may promote Ampkα activity in pancreatic acinar cells. Following adenoviral vector delivery of rat Spef2 (scAAV6.Spef2) or a negative control (scAAV6.Ctrl) under the control of the rat elastase I promoter to enable pancreatic acinar cell-specific Spef2 overexpression, we conducted immunoblotting and Ampkα activity assays in scAAV6.Ctrl AR42J cells and scAAV6.Spef2 AR42J cells. We confirmed Spef2 messenger RNA (mRNA) and protein overexpression in scAAV6.Spef2 AR42J cells (Figure S3C,S3D). We also found that Spef2 overexpression by scAAV6.Spef2 significantly increased Ampkα^{Thr172} phosphorylation (Figure S3D,S3E) and Ampkα activity (Figure S3F) in AR42J whole cell lysates.

Pancreatic acinar cell-specific Spef2 overexpression attenuates acute pancreatitis and associated lung injury in vivo

As Spef2 is downregulated in acute pancreatitis (43,44) and Spef2 promotes Ampkα activation *in vitro*, we hypothesized that Spef2 overexpression in pancreatic acinar cells *in vivo* would offer a protective role against acute pancreatitis and associated lung injury. Therefore, we performed an *in vivo* experiment using scAAV6.Spef2 or scAAV6.Ctrl to enable acinar cell-specific Spef2 overexpression.

As with the previous experimental series, we assessed pancreatic injury 24 hours post-treatment. We confirmed scAAV6-driven pancreatic Spef2 overexpression by quantitative polymerase chain reaction (qPCR; Figure S4). Hematoxylin and eosin (H&E) staining and pathological scoring of pancreatic tissue (*Figure 2A*,*2B*); pancreatic LDH, MDA, LPO, and MPO assays (*Figure 2C*); pancreatic ATP levels (*Figure 2D*); pancreatic necrosis levels (*Figure 2E*); pancreatic apoptosis levels (Figure S5); immunoblotting of Spef2 and Ampkα/Sirt1/NF-κB signaling proteins (*Figure 2F* and Figure S6); and serum levels of inflammatory mediators (*Figure 2G*) revealed that Spef2 overexpression offered a protective role in acute pancreatitis *in vivo*. In addition, assessment of acute pancreatitis-associated lung injury 24 hours post-treatment revealed that Spef2 overexpression offered a protective role in acute pancreatitis-associated lung injury *in vivo* (*Figure 2H-2M*).

Spef2's suppressive effect on in vitro pancreatic acinar cell death and inflammation mediated via the Ampkα/Sirt1 axis

As Spef2 promotes Ampkα activation *in vitro* and offers a protective role in acute pancreatitis and associated lung injury *in vivo*, we hypothesized that Spef2's effects may be mediated through the Ampkα/Sirt1 axis. Therefore, we conducted a series of *in vitro* rescue studies involving delivery of scAAV6.Spef2 (for Spef2 overexpression), siAmpkα (for Ampkα silencing), and/or scAAV6.CA-Sirt1 [for constitutively active (CA)-Sirt1 overexpression] to cerulein-treated AR42J cells. We confirmed scAAV6-driven Spef2 and Sirt1 mRNA overexpression by qPCR as well as Ampkα mRNA silencing by siAmpkα in AR42J cells (Figure S7). We also demonstrated that protein levels of Spef2 were higher in cerulein + scAAV6.Spef2 + siCtrl AR42J cells than in cerulein + scAAV6.NC + siCtrl AR42J cells. Moreover, the cerulein + scAAV6.Spef2 + siAmpkα AR42J cells had significantly reduced protein levels of Ampkα and Sirt1 when compared to the cerulein + scAAV6.Spef2 + siCtrl AR42J cells. We also demonstrated that protein levels of Sirt1 were restored in cerulein + scAAV6.Spef2+ CA-Sirt1 + siAmpkα AR42J cells (*Figure 3A* and Figure S8).

Consistent with our *in vivo* observations, Ampkα^{Thr172} phosphorylation and Sirt1 expression were downregulated while NF-κB p65 phosphorylation, TNF-α expression, and IL-1β expression were upregulated in cerulein-treated AR42J cells compared to in control cells (*Figure 3A* and Figure S8). Spef2 overexpression enhanced Ampkα^{Thr172}

© Annals of Translational Medicine. All rights reserved.

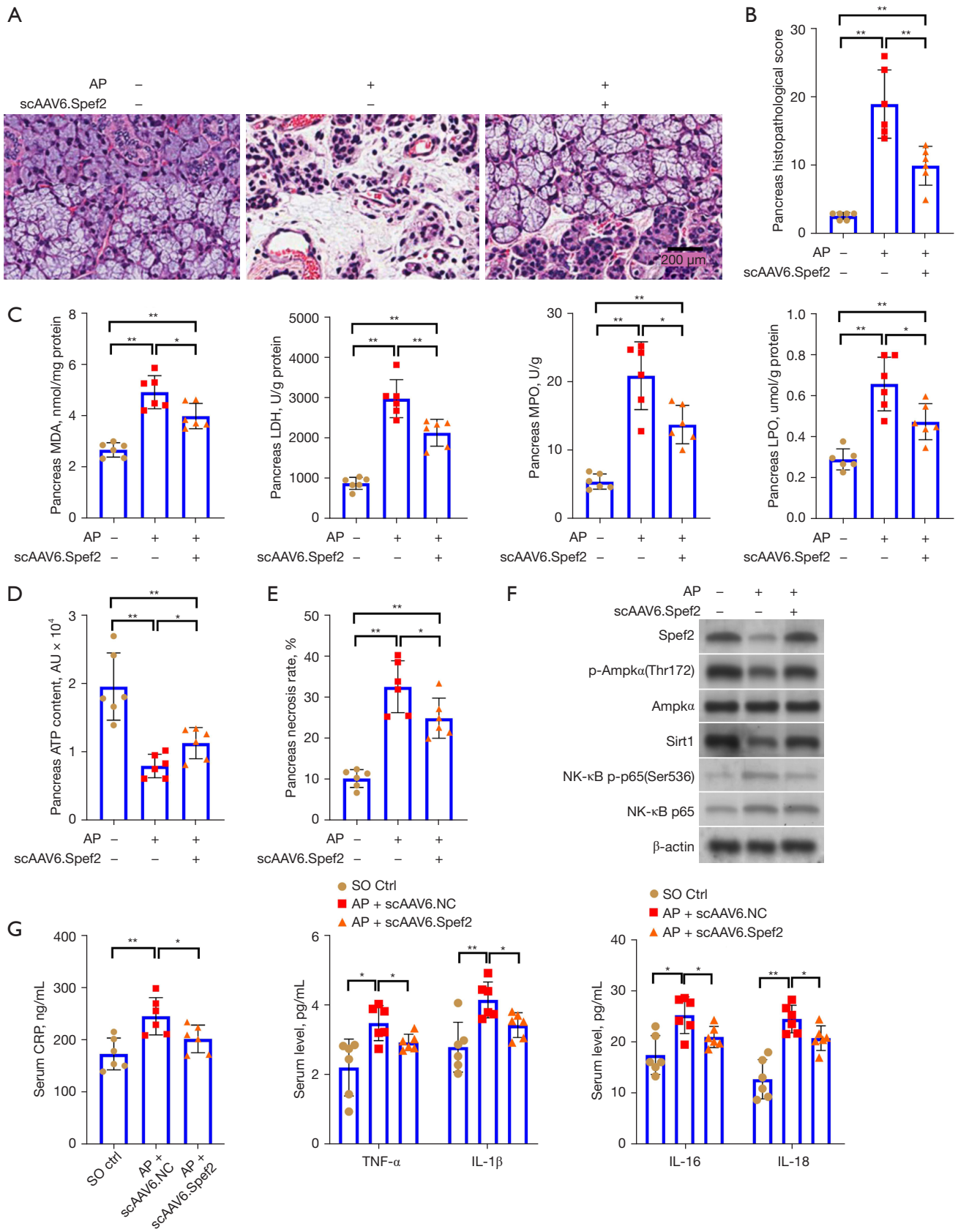

© Annals of Translational Medicine. All rights reserved.

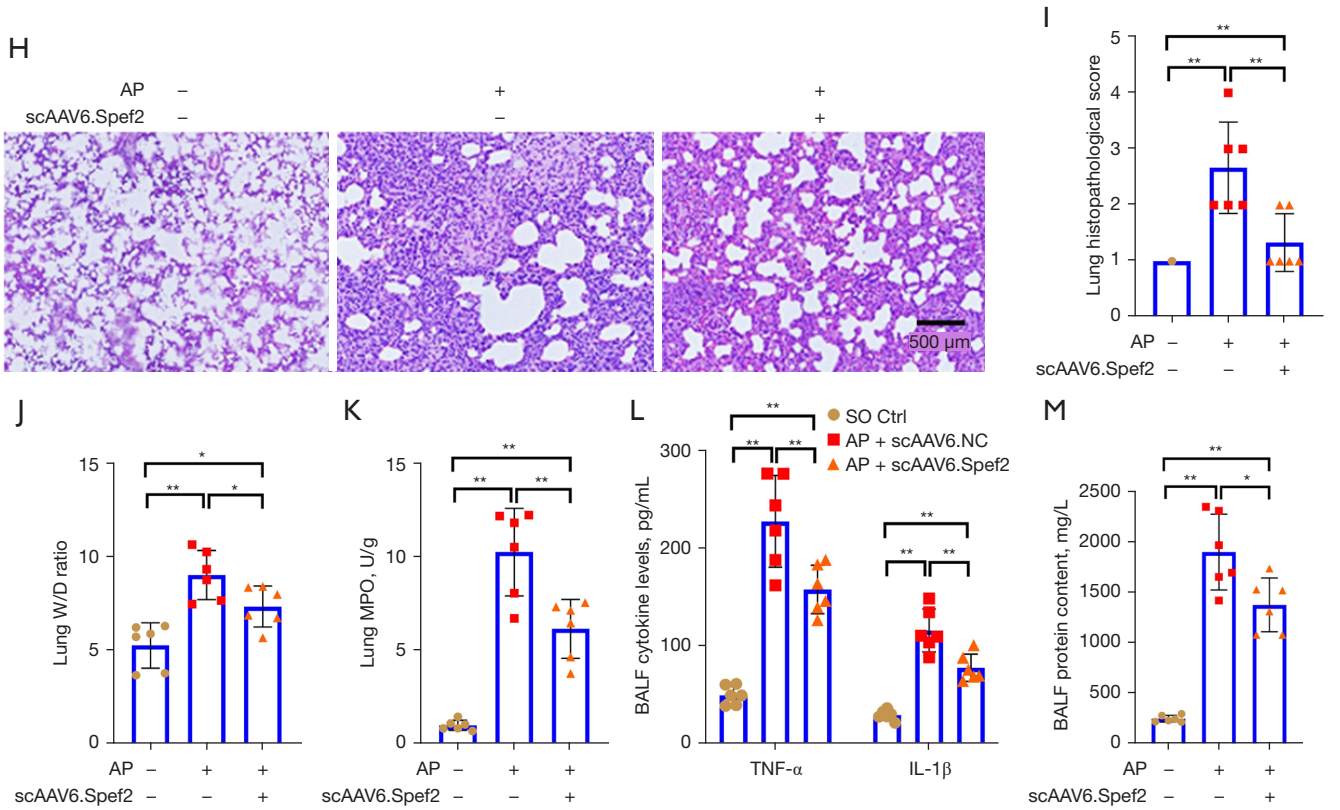

Figure 2 Pancreatic acinar cell-specific Spef2 overexpression attenuates acute pancreatitis and associated lung injury *in vivo*. Pancreatic and lung tissues and peripheral blood samples were harvested from sham-operated control (SO Ctrl), acute pancreatitis + DMSO vehicle (AP + Veh), and acute pancreatitis + scAAV6-delivered Spef2 (AP + scAAV6.Spef2) rats 24 hours post-induction. (A) Representative H&E staining of pancreatic tissues. (B) Pathological scoring of pancreatic injury. (C) Pancreatic LDH, MDA, LPO, and MPO activity levels. (D) Pancreatic ATP levels. (E) Pancreatic necrosis levels. (F) Representative immunoblots of pancreatic Spef2 and Ampkα/Sirt1/NF-κB signaling proteins. (G) Serum CRP, TNF-α, IL-1β, IL-6, and IL-18 levels from peripheral blood samples. (H) H&E staining of lung tissue showing extensive edema, alveolar congestion, and immune cell infiltration (scale bar =500 μm). (I) Pathological scoring of lung tissue injury. (J) Lung W/D ratio. (K) Lung MPO activity. (L) BALF TNF-α and IL-1β levels and (M) BALF protein content. Data represented as means ± SDs. N=6 rats per cohort. *P<0.05, **P<0.01 (one-way ANOVA with Bonferroni post-hoc). Spef2, sperm flagellar 2; DMSO, dimethyl sulfoxide; H&E, hematoxylin and eosin; LDH, lactate dehydrogenase; MDA, malondialdehyde; LPO, lipid peroxide; MPO, myeloperoxidase; ATP, adenosine triphosphate; Ampkα, adenosine monophosphate-activated protein kinase alpha; Sirt1, sirtuin 1; NF-κB, nuclear factor kappa B; CRP, C-reactive protein; TNF-α, tumor necrosis factor alpha; IL-1β, interleukin-1 beta; W/D, wet-to-dry; BALF, bronchoalveolar lavage fluid; SD, standard deviation; ANOVA, analysis of variance.

phosphorylation and Sirt1 expression and reduced NF-κB p65 phosphorylation in cerulein-treated AR42J cells (*Figure 3A* and Figure S8). Addition of siAmpkα to Spef2 overexpression AR42J cells knocked-down Ampkα^{Thr172} phosphorylation and Sirt1 expression and enhanced NF-κB p65 phosphorylation. Addition of CA-Sirt1 overexpression to the above cells rescued the effects of siAmpkα and restored Spef2's downregulation of NF-κB p65 phosphorylation.

LDH assays (*Figure 3B*), ATP assays (*Figure 3C*), necrosis assays (*Figure 3D*), TUNEL and CC-3 staining assays (*Figure 3E-3H*), and inflammatory mediator release assays (*Figure 3I*) revealed that cerulein-treated AR42J cells showed greater oxidative stress, necrosis, apoptosis, and inflammation compared to control cells. Spef2 overexpression reduced these effects in cerulein-treated AR42J cells (*Figure 3B-3I*). Addition of siAmpkα to Spef2 overexpression AR42J cells enhanced these effects, while

© Annals of Translational Medicine. All rights reserved.

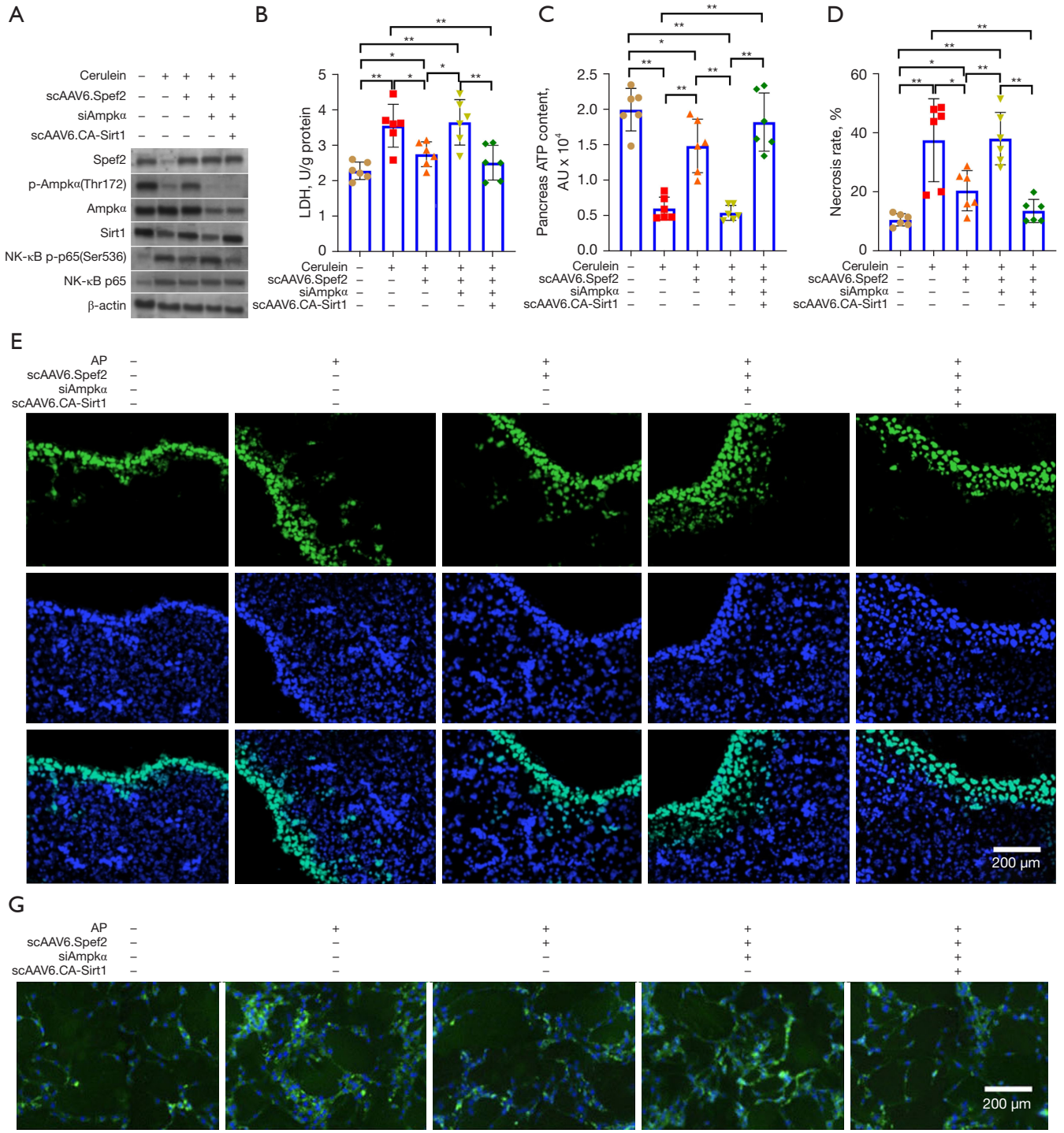

© Annals of Translational Medicine. All rights reserved.

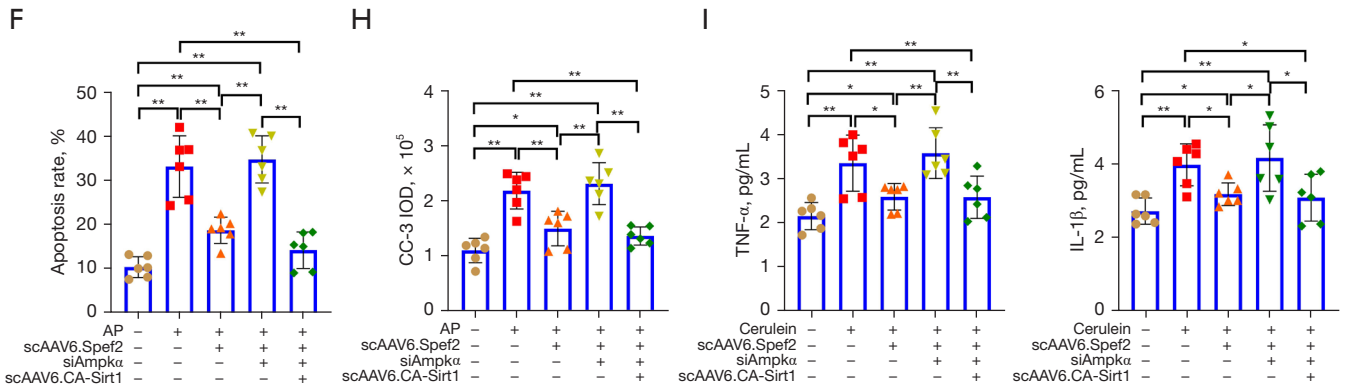

Figure 3 Spef2's suppressive effect on *in vitro* pancreatic acinar cell necrosis and inflammation mediated via the Ampkα/Sirt1 axis. 72 hours following scAAV6.NC, scAAV6.Spef2, or scAAV6.Spef2 + CA-Sirt1 infection and 12 hours following siCtrl or siAmpkα transfection, AR42J cells were incubated with cerulein to establish an *in vitro* model of acute pancreatitis. (A) Representative immunoblots of pancreatic Spef2 and Ampkα/Sirt1/NF-κB signaling proteins. (B) LDH levels. (C) ATP levels. (D) Cell necrosis levels. (E) Representative TUNEL staining images and (F) associated quantitative measurements of apoptosis. (G) Representative CC-3 fluorescent staining images. CC-3 staining in green and DAPI nuclei staining in blue (scale bar =200 μm). (H) IOD quantitation of fluorescent CC-3 staining. (I) Cell supernatant TNF-α and IL-1β levels. Data represented as means ± SDs. N=3 biological replicates × 2 technical replicates. *P<0.05, **P<0.01 (one-way ANOVA with Bonferroni post-hoc). Spef2, sperm flagellar 2; Ampkα, adenosine monophosphate-activated protein kinase alpha; Sirt1, sirtuin 1; CA, constitutively active; NF-κB, nuclear factor kappa B; LDH, lactate dehydrogenase; ATP, adenosine triphosphate; TUNEL, terminal deoxynucleotidyl transferase dUTP nick end labeling; CC-3, cleaved caspase-3; DAPI, 4',6-diamidino-2-phenylindole; TNF-α, tumor necrosis factor alpha; IL-1β, interleukin-1 beta; SD, standard deviation; ANOVA, analysis of variance; IOD, integrated optical density.

addition of CA-Sirt1 overexpression to these cells rescued the effects of siAmpkα and restored Spef2's downregulation of oxidative stress, necrosis, apoptosis, and inflammation (*Figure 3B-3I*). In sum, Spef2's suppressive effect on *in vitro* pancreatic acinar cell necrosis and inflammation is mediated via the Ampkα/Sirt1 axis.

Spef2's suppressive effect on in vivo acute pancreatitis and associated lung injury mediated via the Ampkα/Sirt1 axis

Having shown that Spef2's suppressive effect on acinar cell necrosis and inflammation is Ampkα/Sirt1 axis-mediated, we performed an additional rodent experiment to confirm this phenomenon *in vivo*. Therefore, we conducted a series of *in vivo* rescue studies involving delivery of scAAV6.Spef2 (for Spef2 overexpression), siAmpkα (for Ampkα silencing), and/or scAAV6.CA-Sirt1 (for CA-Sirt1 overexpression) to acute pancreatitis rats.

As with the previous *in vivo* experimental series, we assessed pancreatic injury 24 hours post-treatment. We confirmed scAAV6-driven Spef2 and Sirt1 mRNA overexpression by qPCR as well as Ampkα mRNA silencing by siAmpkα in pancreatic tissue (Figure S9). H&E staining and pathological scoring of pancreatic tissue (*Figure 4A,4B*); pancreatic LDH, MDA, LPO, and MPO assays (*Figure 4C*); pancreatic ATP levels (*Figure 4D*); pancreatic necrosis levels (*Figure 4E*); pancreatic apoptosis levels (Figure S10); immunoblotting of Spef2 and Ampkα/Sirt1/NF-κB signaling proteins (*Figure 4F* and Figure S11); and serum levels of inflammatory mediators (*Figure 4G*) revealed that Spef2's protective role in acute pancreatitis is Ampkα/Sirt1 axis–mediated. In addition, assessment of acute pancreatitis–associated lung injury 24 hours post-treatment revealed that Spef2's protective role in acute pancreatitis is Ampkα/Sirt1 axis-mediated (*Figure 4H-4M*).

Discussion

The pathological changes of early acute pancreatitis occur in acinar cells (49). Mild and severe acute pancreatitis share several common acinar cell characteristics; however, disease severity and prognosis differ greatly between the two. The response to the initial intracellular damage becomes a vital factor in determining the extent of inflammation, which influences the development of either mild or severe acute pancreatitis. Specifically, mild

© Annals of Translational Medicine. All rights reserved.

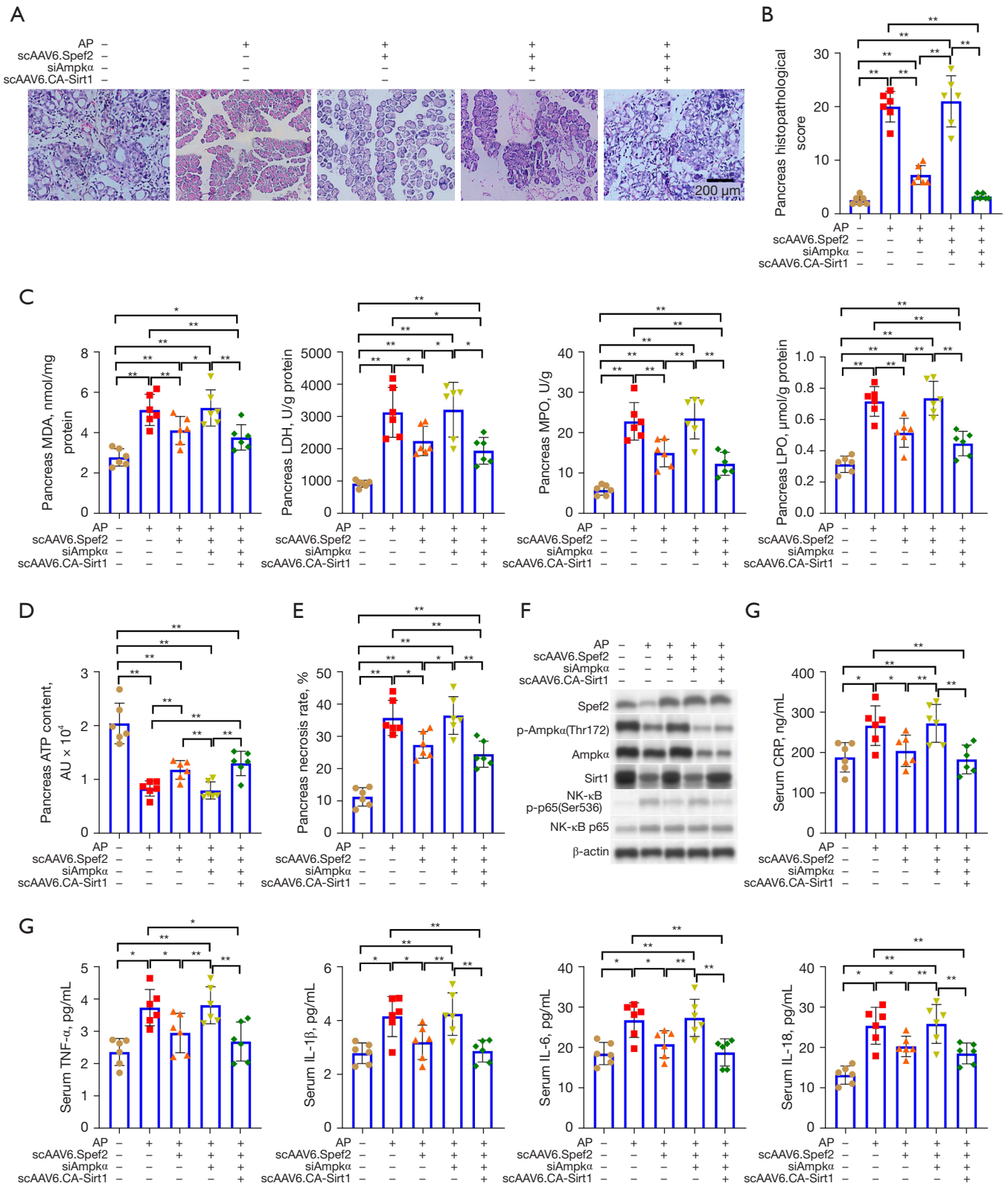

© Annals of Translational Medicine. All rights reserved.

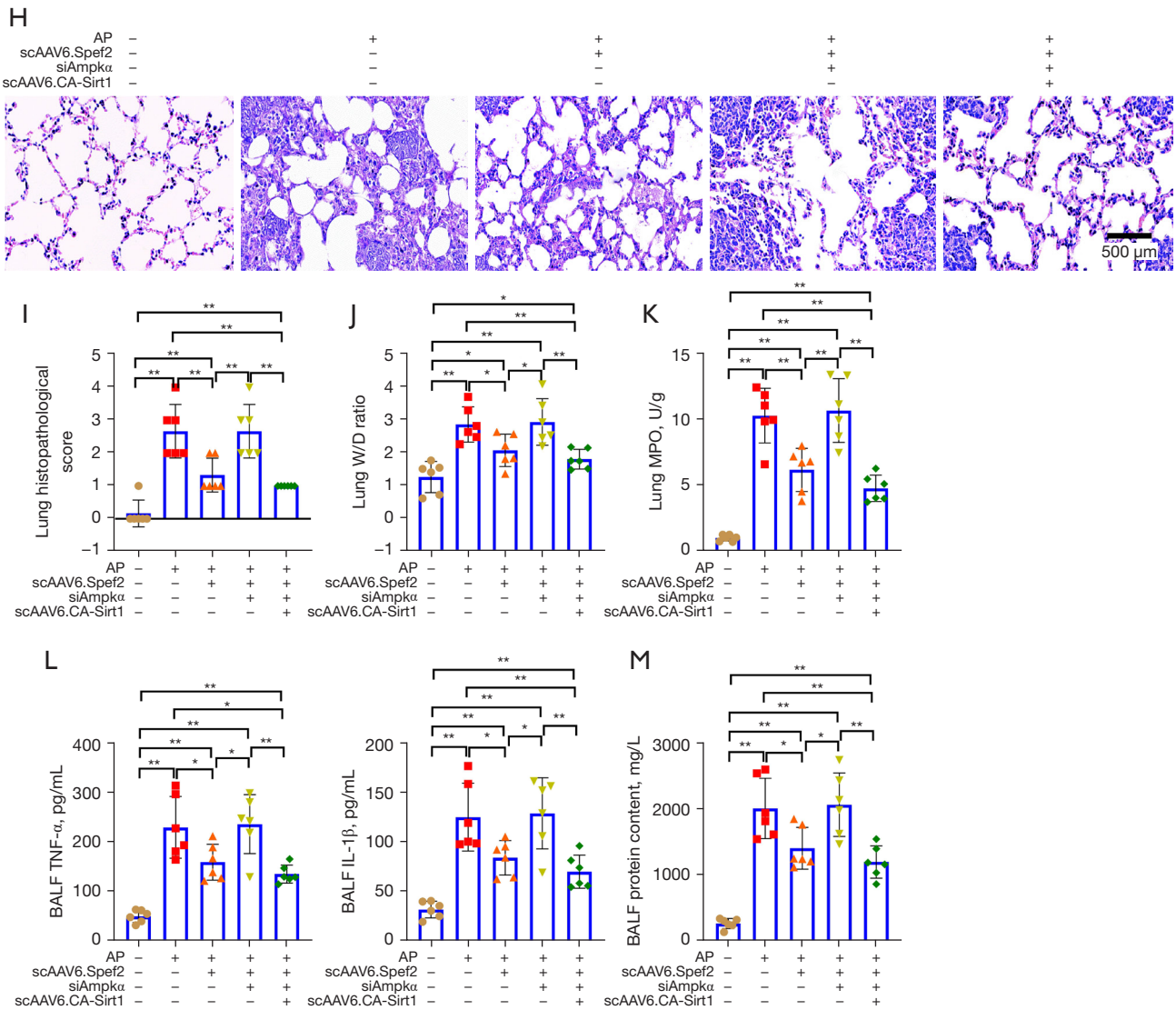

Figure 4 Spef2's suppressive effect on *in vivo* acute pancreatitis and associated lung injury mediated via the Ampkα/Sirt1 axis. Pancreatic and lung tissues and peripheral blood samples were harvested from sham-operated control (SO Ctrl), acute pancreatitis + DMSO vehicle (AP + Veh), acute pancreatitis + scAAV6-delivered Spef2 + control siRNA (AP + scAAV6.Spef2 + siCtrl), acute pancreatitis + scAAV6-delivered Spef2 + Ampkα siRNA (AP + scAAV6.Spef2 + siAmpkα), and acute pancreatitis + scAAV6-delivered Spef2 + Ampkα siRNA + scAAV6-delivered CA-Sirt1 (AP + scAAV6.Spef2 + CA-Sirt1 + siAmpkα) rats 24 hours post-induction. (A) Representative H&E staining of pancreatic tissues. (B) Pathological scoring of pancreatic injury. (C) Pancreatic LDH, MDA, LPO, and MPO activity levels. (D) Pancreatic ATP levels. (E) Pancreatic necrosis levels. (F) Representative immunoblots of pancreatic Spef2 and Ampkα/Sirt1/NF-κB signaling proteins. (G) Serum CRP, TNF-α, IL-1β, IL-6, and IL-18 levels from peripheral blood samples. (H) H&E staining of lung tissue showing extensive edema, alveolar congestion, and immune cell infiltration (scale bar =500 μm). (I) Pathological scoring of lung tissue injury. (J) Lung W/D ratio. (K) Lung MPO activity. (L) BALF TNF-α and IL-1β levels and (M) BALF protein content. Data represented as means ± SDs. N=6 rats per cohort. *P<0.05, **P<0.01 (one-way ANOVA with Bonferroni post-hoc). Spef2, sperm flagellar 2; Ampkα, adenosine monophosphate-activated protein kinase alpha; Sirt1, sirtuin 1; DMSO, dimethyl sulfoxide; siRNA, small-interfering RNA; CA, constitutively active; H&E, hematoxylin and eosin; LDH, lactate dehydrogenase; MDA, malondialdehyde; LPO, lipid peroxide; MPO, myeloperoxidase; ATP, adenosine triphosphate; NF-κB, nuclear factor kappa B; CRP, C-reactive protein; TNF-α, tumor necrosis factor alpha; IL-1β, interleukin-1 beta; W/D, wet-to-dry; BALF, bronchoalveolar lavage fluid; SD, standard deviation; ANOVA, analysis of variance.

© Annals of Translational Medicine. All rights reserved.

acute pancreatitis is predominantly characterized by mild inflammation and acinar cell apoptosis, whereas severe acute pancreatitis is predominantly characterized by higher levels of inflammation and acinar cell necrosis (50). Disease mortality in acute pancreatitis patients is strongly associated with the degree of tissue necrosis, as patients with detectable necrosis levels of greater than 50% have a significantly higher mortality rate (51). As acinar cell necrosis is a rapid process (23), the ability to quickly reduce or prevent inflammation during early acute pancreatitis could limit acinar cell necrosis and overall disease progression.

Here, we first investigated the role of Ampkα on acinar cell necrosis, apoptosis, and inflammation in a rodent model of acute pancreatitis and associated lung injury. The serine/threonine kinase Ampkα negatively regulates pro-inflammatory NF-κB activity (46). In our *in vivo* rodent model, pharmacological Ampkα activation with the thienopyridone derivative A769662 (52) reduced acute pancreatitis severity, oxidative stress, necrosis, apoptosis, NF-kB-mediated inflammation, and the degree of associated lung injury. This is consistent with numerous previous studies showing the anti-inflammatory effects of Ampkα agonism in other animal models of inflammatory disease, including inflammatory liver fibrosis (53), cardiac inflammation (54), amyloid-β-induced neuroinflammation (55), adipose tissue inflammation (56), inflammation-driven muscle atrophy (57), and synovial tissue inflammation (58). Previous molecular research reports that Ampkα's negative regulation of NF-κB activity operates through its downstream intermediaries Sirt1, forkhead box O (Foxo), and peroxisome proliferator-activated receptor gamma coactivator 1-alpha (Pgc1α) (46). Accordingly, we found that pharmacological Ampkα activation stimulated anti-inflammatory Sirt1 upregulation in acinar cells.

Ampkα activity is regulated through a myriad of mechanisms, most notably the allosteric activation of the enzyme by the intracellular messenger molecule AMP (from which Ampkα derives its name) (59). Therefore, enzymes that regulate intracellular AMP levels—such as ADK, AK, AMP deaminase (AMPD), and 5'-nucleotidases (NT5Cs)—can have profound effects upon Ampkα activity (60,61). Here, we found that the ciliary protein Spef2—which contains an AK domain (47)—promotes Ampkα activity in acinar cells and is downregulated in acute pancreatitis. Therefore, we postulated the existence of a Spef2/Ampkα/Sirt1 axis and hypothesized that this axis may be involved in the regulation of NF-κB-mediated acinar cell inflammation and resulting cell necrosis during acute pancreatitis. To test this hypothesis, we conducted a series of *in vitro* and *in vivo* rescue studies involving delivery of scAAV6.Spef2 (for Spef2 overexpression), siAmpkα (for Ampkα silencing), and/or scAAV6.CA-Sirt1 (for CA-Sirt1 overexpression). Indeed, we found that Spef2's suppressive effect on acute pancreatitis and associated lung injury is mediated via the Ampkα/Sirt1 axis. Our findings are consistent with previous research supporting the anti-NF-κB-mediated inflammatory effects of Ampkα/Sirt1 signaling (62-64).

To conclude, this study established the existence of a Spef2/Ampkα/Sirt1 axis in pancreatic acinar cells that is involved in the regulation of NF-κB-mediated acinar cell inflammation and resulting cell necrosis during acute pancreatitis. We found that the ciliary protein Spef2 suppressed acute pancreatitis and associated lung injury via activating the Ampkα/Sirt1 axis, and Spef2 could be a potential biomarker for the prevention, diagnosis, and treatment of acute pancreatitis-induced lung injury. Further work is needed to fully elucidate the etiology of acinar cell Spef2 downregulation in acute pancreatitis and the precise mechanism(s) of action underlying Spef2's effects on Ampkα activity in acinar cells.

Acknowledgments

Funding: This study was supported by grants from the Nature Science Foundation of Fujian, China (Nos. 2018J01215 and 2020J011338) and the Science and Technology Plan Projects Foundation of Ningde, China (No. 20170110).

Footnote

Reporting Checklist: The authors have completed the ARRIVE reporting checklist. Available at https://atm.amegroups.com/article/view/10.21037/atm-22-3118/rc

Data Sharing Statement: Available at https://atm.amegroups.com/article/view/10.21037/atm-22-3118/dss

Conflicts of Interest: All authors have completed the ICMJE uniform disclosure form (available at https://atm.amegroups.com/article/view/10.21037/atm-22-3118/coif). The authors have no conflicts of interest to declare.

Ethical Statement: The authors are accountable for all

© Annals of Translational Medicine. All rights reserved.

aspects of the work in ensuring that questions related to the accuracy or integrity of any part of the work are appropriately investigated and resolved. Institutional approval for this study was obtained in advance from the Ethics Committee of Mindong Hospital Affiliated to Fujian Medical University (Fu'an, China; No. 20200126K). All animal experiments were conducted in accordance with the National Institutes of Health (NIH) Guide for the Care and Use of Laboratory Animals (Bethesda, MD, USA).

Open Access Statement: This is an Open Access article distributed in accordance with the Creative Commons Attribution-NonCommercial-NoDerivs 4.0 International License (CC BY-NC-ND 4.0), which permits the non-commercial replication and distribution of the article with the strict proviso that no changes or edits are made and the original work is properly cited (including links to both the formal publication through the relevant DOI and the license). See: https://creativecommons.org/licenses/by-nc-nd/4.0/.

References

1. Pandol SJ, Saluja AK, Imrie CW, et al. Acute pancreatitis: bench to the bedside. Gastroenterology 2007;132:1127-51.
2. Peery AF, Crockett SD, Murphy CC, et al. Burden and Cost of Gastrointestinal, Liver, and Pancreatic Diseases in the United States: Update 2018. Gastroenterology 2019;156:254-272.e11.
3. Moggia E, Koti R, Belgaumkar AP, et al. Pharmacological interventions for acute pancreatitis. Cochrane Database Syst Rev 2017;4:CD011384.
4. Banks PA, Bollen TL, Dervenis C, et al. Classification of acute pancreatitis--2012: revision of the Atlanta classification and definitions by international consensus. Gut 2013;62:102-11.
5. Vege SS, DiMagno MJ, Forsmark CE, et al. Initial Medical Treatment of Acute Pancreatitis: American Gastroenterological Association Institute Technical Review. Gastroenterology 2018;154:1103-39.
6. Shah AP, Mourad MM, Bramhall SR. Acute pancreatitis: current perspectives on diagnosis and management. J Inflamm Res 2018;11:77-85.
7. Huang H, Liu Y, Daniluk J, et al. Activation of nuclear factor-κB in acinar cells increases the severity of pancreatitis in mice. Gastroenterology 2013;144:202-10.
8. Dumnicka P, Maduzia D, Ceranowicz P, et al. The Interplay between Inflammation, Coagulation and Endothelial Injury in the Early Phase of Acute Pancreatitis: Clinical Implications. Int J Mol Sci 2017;18:354.
9. De Campos T, Deree J, Coimbra R. From acute pancreatitis to end-organ injury: mechanisms of acute lung injury. Surg Infect (Larchmt) 2007;8:107-20.
10. Zhou MT, Chen CS, Chen BC, et al. Acute lung injury and ARDS in acute pancreatitis: mechanisms and potential intervention. World J Gastroenterol 2010;16:2094-9.
11. Lomas-Neira J, Chung CS, Perl M, et al. Role of alveolar macrophage and migrating neutrophils in hemorrhage-induced priming for ALI subsequent to septic challenge. Am J Physiol Lung Cell Mol Physiol 2006;290:L51-8.
12. Sailai Y, Yu X, Baiheti P, et al. Influence of nuclear factor kappaB activation on inflammatory mediators of alveolar macrophages in rats with acute necrotizing pancreatitis. J Investig Med 2010;58:38-42.
13. Hardie DG. AMP-activated/SNF1 protein kinases: conserved guardians of cellular energy. Nat Rev Mol Cell Biol 2007;8:774-85.
14. Steinberg GR, Michell BJ, van Denderen BJ, et al. Tumor necrosis factor alpha-induced skeletal muscle insulin resistance involves suppression of AMP-kinase signaling. Cell Metab 2006;4:465-74.
15. Ko HJ, Zhang Z, Jung DY, et al. Nutrient stress activates inflammation and reduces glucose metabolism by suppressing AMP-activated protein kinase in the heart. Diabetes 2009;58:2536-46.
16. Carroll KC, Viollet B, Suttles J. AMPKα1 deficiency amplifies proinflammatory myeloid APC activity and CD40 signaling. J Leukoc Biol 2013;94:1113-21.
17. Fulco M, Cen Y, Zhao P, et al. Glucose restriction inhibits skeletal myoblast differentiation by activating SIRT1 through AMPK-mediated regulation of Nampt. Dev Cell 2008;14:661-73.
18. Cantó C, Auwerx J. PGC-1alpha, SIRT1 and AMPK, an energy sensing network that controls energy expenditure. Curr Opin Lipidol 2009;20:98-105.
19. Chyau CC, Wang HF, Zhang WJ, et al. Antrodan Alleviates High-Fat and High-Fructose Diet-Induced Fatty Liver Disease in C57BL/6 Mice Model via AMPK/Sirt1/SREBP-1c/PPARγ Pathway. Int J Mol Sci 2020;21:360.
20. Yang J, Zhou Y, Shi J. Cordycepin protects against acute pancreatitis by modulating NF-κB and NLRP3 inflammasome activation via AMPK. Life Sci 2020;251:117645.
21. Bi Y, Ji B. Spontaneous pancreatitis in genetically modified animal strains. Pancreapedia: The Exocrine Pancreas Knowledge Base. 2016.
22. Quirin KA, Kwon JJ, Alioufi A, et al. Safety and Efficacy

© Annals of Translational Medicine. All rights reserved.

of AAV Retrograde Pancreatic Ductal Gene Delivery in Normal and Pancreatic Cancer Mice. Mol Ther Methods Clin Dev 2018;8:8-20.
23. Ji L, Li L, Qu F, et al. Hydrogen sulphide exacerbates acute pancreatitis by over-activating autophagy via AMPK/mTOR pathway. J Cell Mol Med 2016;20:2349-61.
24. Bai X, Song Z, Zhou Y, et al. The apoptosis of peripheral blood lymphocytes promoted by hyperbaric oxygen treatment contributes to attenuate the severity of early stage acute pancreatitis in rats. Apoptosis 2014;19:58-75.
25. Lv JC, Wang G, Pan SH, et al. Lycopene protects pancreatic acinar cells against severe acute pancreatitis by abating the oxidative stress through JNK pathway. Free Radic Res 2015;49:151-63.
26. Wang G, Sun B, Gao Y, et al. The effect of emodin-assisted early enteral nutrition on severe acute pancreatitis and secondary hepatic injury. Mediators Inflamm 2007;2007:29638.
27. Wang G, Sun B, Zhu H, et al. Protective effects of emodin combined with danshensu on experimental severe acute pancreatitis. Inflamm Res 2010;59:479-88.
28. Mo J, Yang A, Chen Z, et al. Neuronostatin ameliorates sodium taurocholate-induced acute pancreatitis in rats. Dig Dis Sci 2013;58:2903-7.
29. Mittal A, Hickey AJ, Chai CC, et al. Early organ-specific mitochondrial dysfunction of jejunum and lung found in rats with experimental acute pancreatitis. HPB (Oxford) 2011;13:332-41.
30. Barreto-Torres G, Javadov S. Possible Role of Interaction between PPARα and Cyclophilin D in Cardioprotection of AMPK against In Vivo Ischemia-Reperfusion in Rats. PPAR Res 2016;2016:9282087.
31. Kusske AM, Rongione AJ, Ashley SW, et al. Interleukin-10 prevents death in lethal necrotizing pancreatitis in mice. Surgery 1996;120:284-8; discussion 289.
32. Osman MO, Kristensen JU, Jacobsen NO, et al. A monoclonal anti-interleukin 8 antibody (WS-4) inhibits cytokine response and acute lung injury in experimental severe acute necrotising pancreatitis in rabbits. Gut 1998;43:232-9.
33. Duprez L, Takahashi N, Van Hauwermeiren F, et al. RIP kinase-dependent necrosis drives lethal systemic inflammatory response syndrome. Immunity 2011;35:908-18.
34. Marcinkiewicz J, Grabowska A, Bereta J, et al. Taurine chloramine down-regulates the generation of murine neutrophil inflammatory mediators. Immunopharmacology 1998;40:27-38.
35. Moriwaki K, Balaji S, McQuade T, et al. The necroptosis adaptor RIPK3 promotes injury-induced cytokine expression and tissue repair. Immunity 2014;41:567-78.
36. Xiao X, Jones G, Sevilla WA, et al. A Carboxyl Ester Lipase (CEL) Mutant Causes Chronic Pancreatitis by Forming Intracellular Aggregates That Activate Apoptosis. J Biol Chem 2016;291:23224-36.
37. Lee CT, Ussher JR, Mohammad A, et al. 5'-AMP-activated protein kinase increases glucose uptake independent of GLUT4 translocation in cardiac myocytes. Can J Physiol Pharmacol 2014;92:307-14.
38. Crowley LC, Marfell BJ, Scott AP, et al. Quantitation of Apoptosis and Necrosis by Annexin V Binding, Propidium Iodide Uptake, and Flow Cytometry. Cold Spring Harb Protoc 2016.
39. Li L, Chen H, Gao Y, et al. Long Noncoding RNA MALAT1 Promotes Aggressive Pancreatic Cancer Proliferation and Metastasis via the Stimulation of Autophagy. Mol Cancer Ther 2016;15:2232-43.
40. Wang G, Han B, Zhou H, et al. Inhibition of hydrogen sulfide synthesis provides protection for severe acute pancreatitis rats via apoptosis pathway. Apoptosis 2013;18:28-42.
41. Kong R, Sun B, Jiang H, et al. Downregulation of nuclear factor-kappaB p65 subunit by small interfering RNA synergizes with gemcitabine to inhibit the growth of pancreatic cancer. Cancer Lett 2010;291:90-8.
42. Zhong M, Zhao X, Li J, et al. Tumor Suppressor Folliculin Regulates mTORC1 through Primary Cilia. J Biol Chem 2016;291:11689-97.
43. Reichert M, Takano S, von Burstin J, et al. The Prrx1 homeodomain transcription factor plays a central role in pancreatic regeneration and carcinogenesis. Genes Dev 2013;27:288-300.
44. Norberg KJ, Nania S, Li X, et al. RCAN1 is a marker of oxidative stress, induced in acute pancreatitis. Pancreatology 2018;18:734-41.
45. Jarvis MF. Therapeutic potential of adenosine kinase inhibition-Revisited. Pharmacol Res Perspect 2019;7:e00506.
46. Jeon SM. Regulation and function of AMPK in physiology and diseases. Exp Mol Med 2016;48:e245.
47. Liu W, Sha Y, Li Y, et al. Loss-of-function mutations in SPEF2 cause multiple morphological abnormalities of the sperm flagella (MMAF). J Med Genet 2019;56:678-84.
48. Dzeja P, Terzic A. Adenylate kinase and AMP signaling networks: metabolic monitoring, signal communication and body energy sensing. Int J Mol Sci 2009;10:1729-72.

© Annals of Translational Medicine. All rights reserved.

49. Bhatia M, Wong FL, Cao Y, et al. Pathophysiology of acute pancreatitis. Pancreatology 2005;5:132-44.
50. Kaiser AM, Saluja AK, Lu L, et al. Effects of cycloheximide on pancreatic endonuclease activity, apoptosis, and severity of acute pancreatitis. Am J Physiol 1996;271:C982-93.
51. Gadiparthi C, Mohapatra S, Kanna S, et al. Acute pancreatitis in a patient with COVID-19: a case report. Transl Gastroenterol Hepatol 2021;6:65.
52. Scott JW, Ling N, Issa SM, et al. Small molecule drug A-769662 and AMP synergistically activate naive AMPK independent of upstream kinase signaling. Chem Biol 2014;21:619-27.
53. Wang Y, Li C, Gu J, et al. Celastrol exerts anti-inflammatory effect in liver fibrosis via activation of AMPK-SIRT3 signalling. J Cell Mol Med 2020;24:941-53.
54. Koyani CN, Plastira I, Sourij H, et al. Empagliflozin protects heart from inflammation and energy depletion via AMPK activation. Pharmacol Res 2020;158:104870.
55. Chiang MC, Nicol CJ, Cheng YC. Resveratrol activation of AMPK-dependent pathways is neuroprotective in human neural stem cells against amyloid-beta-induced inflammation and oxidative stress. Neurochem Int 2018;115:1-10.
56. Xiong XQ, Geng Z, Zhou B, et al. FNDC5 attenuates adipose tissue inflammation and insulin resistance via AMPK-mediated macrophage polarization in obesity. Metabolism 2018;83:31-41.
57. Hall DT, Griss T, Ma JF, et al. The AMPK agonist 5-aminoimidazole-4-carboxamide ribonucleotide (AICAR), but not metformin, prevents inflammation-associated cachectic muscle wasting. EMBO Mol Med 2018;10:e8307.
58. Wen Z, Jin K, Shen Y, et al. N-myristoyltransferase deficiency impairs activation of kinase AMPK and promotes synovial tissue inflammation. Nat Immunol 2019;20:313-25.
59. Cameron KO, Kurumbail RG. Recent progress in the identification of adenosine monophosphate-activated protein kinase (AMPK) activators. Bioorg Med Chem Lett 2016;26:5139-48.
60. Kviklyte S, Vertommen D, Yerna X, et al. Effects of genetic deletion of soluble 5'-nucleotidases NT5C1A and NT5C2 on AMPK activation and nucleotide levels in contracting mouse skeletal muscles. Am J Physiol Endocrinol Metab 2017;313:E48-E62..
61. Umezawa S, Higurashi T, Nakajima A. AMPK: Therapeutic Target for Diabetes and Cancer Prevention. Curr Pharm Des 2017;23:3629-44.
62. Tian Y, Ma J, Wang W, et al. Resveratrol supplement inhibited the NF-κB inflammation pathway through activating AMPKα-SIRT1 pathway in mice with fatty liver. Mol Cell Biochem 2016;422:75-84.
63. Chen L, Lan Z. Polydatin attenuates potassium oxonate-induced hyperuricemia and kidney inflammation by inhibiting NF-κB/NLRP3 inflammasome activation via the AMPK/SIRT1 pathway. Food Funct 2017;8:1785-92.
64. Jang HM, Han SK, Kim JK, et al. Lactobacillus sakei Alleviates High-Fat-Diet-Induced Obesity and Anxiety in Mice by Inducing AMPK Activation and SIRT1 Expression and Inhibiting Gut Microbiota-Mediated NF-κB Activation. Mol Nutr Food Res 2019;63:e1800978.

(English Language Editor: C. Gourlay)

Cite this article as: Zhang C, Guo DF, Lv GF, Zhang DC, Lin F, Liu JB, Lin JY, Xiao DX. The ciliary protein Spef2 stimulates acinar Ampkα/Sirt1 signaling and ameliorates acute pancreatitis and associated lung injury. Ann Transl Med 2022;10(14):798. doi: 10.21037/atm-22-3118

© Annals of Translational Medicine. All rights reserved.

Supplementary

Table S1 No change in acute pancreatitis or inflammatory markers following ductal delivery of scAAV6 vector

Serum parameter	Day 1 post-injection			Day 3 post-injection		
	SO Ctrl (n=6)	scAAV6 (n=12)	P value [unpaired *t*-test]	SO Ctrl (n=6)	scAAV6 (n=12)	P value [unpaired *t*-test]
Amylase (U/dL)	1558±122	1666±230	0.21	1591±146	1700±274	0.29
Lipase (U/dL)	81.1±12.3	89.4±14.9	0.23	81.4±12.8	86.6±12.5	0.43
Crp (ng/mL)	198.9±27.9	223.1±43.4	0.17	199.4±32.9	215.0±40.0	0.39
Tnf-α (pg/mL)	2.48±0.36	2.74±0.45	0.21	2.46±0.39	2.76±0.62	0.23
Il-1β (pg/mL)	3.29±0.22	3.54±0.70	0.28	3.24±0.14	3.27±0.56	0.90

Data represented as means ± standard deviations (SDs). SO Ctrl, sham-operated control; Tap, trypsinogen activation peptide; Crp, C-reactive protein; Tnf-α, tumor necrosis factor-alpha

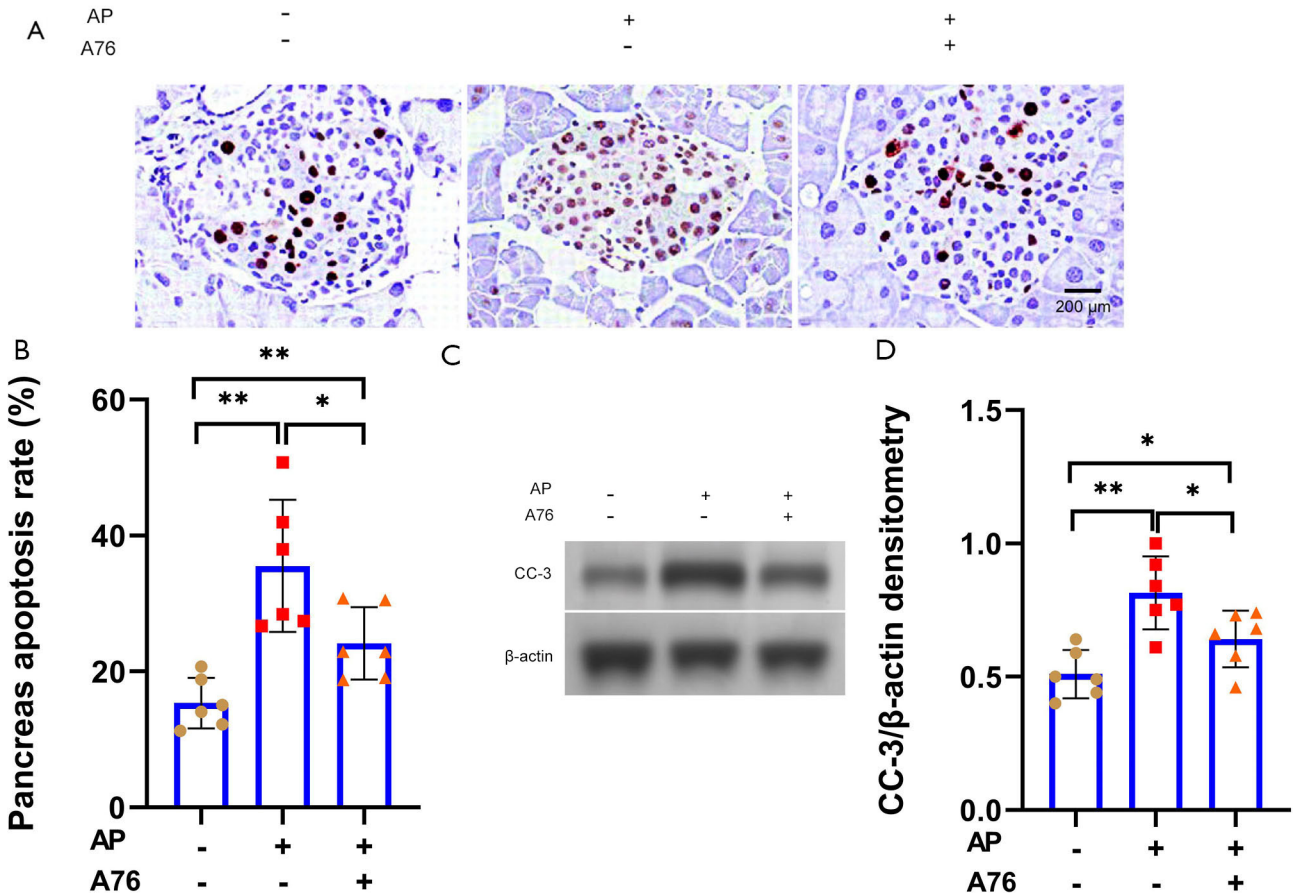

Figure S1 Enhancing Ampkα activity during acute pancreatitis reduces cell apoptosis. (A) Representative TUNEL staining measuring (B) pancreatic cell apoptosis in tissues from the treatment groups described in Figure 1. (C,D) Representative immunoblots and ImageJ densitometric quantitation of pancreatic cleaved caspase-3 (CC-3) expression. Data represented as means ± SDs. N=6 rats per cohort. *P<0.05, **P<0.01 (one-way ANOVA with Bonferroni post-hoc).

© Annals of Translational Medicine. All rights reserved.
https://dx.doi.org/10.21037/atm-22-3118

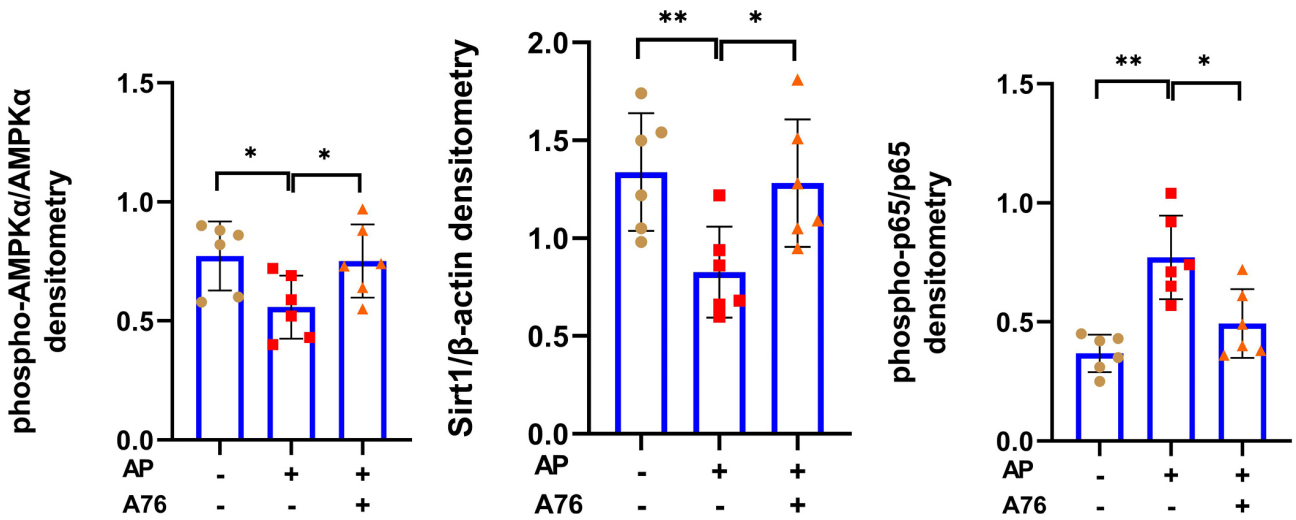

Figure S2 Densitometric analysis of Figure 1F immunoblots. (A-C) Quantitation of pancreatic Ampkα/Sirt1/NF-κB signalling protein expression by ImageJ densitometry. β-actin used as loading control. Data represented as means ± SDs. N=6 rats per cohort. *P<0.05, **P<0.01 (one-way ANOVA with Bonferroni post-hoc).

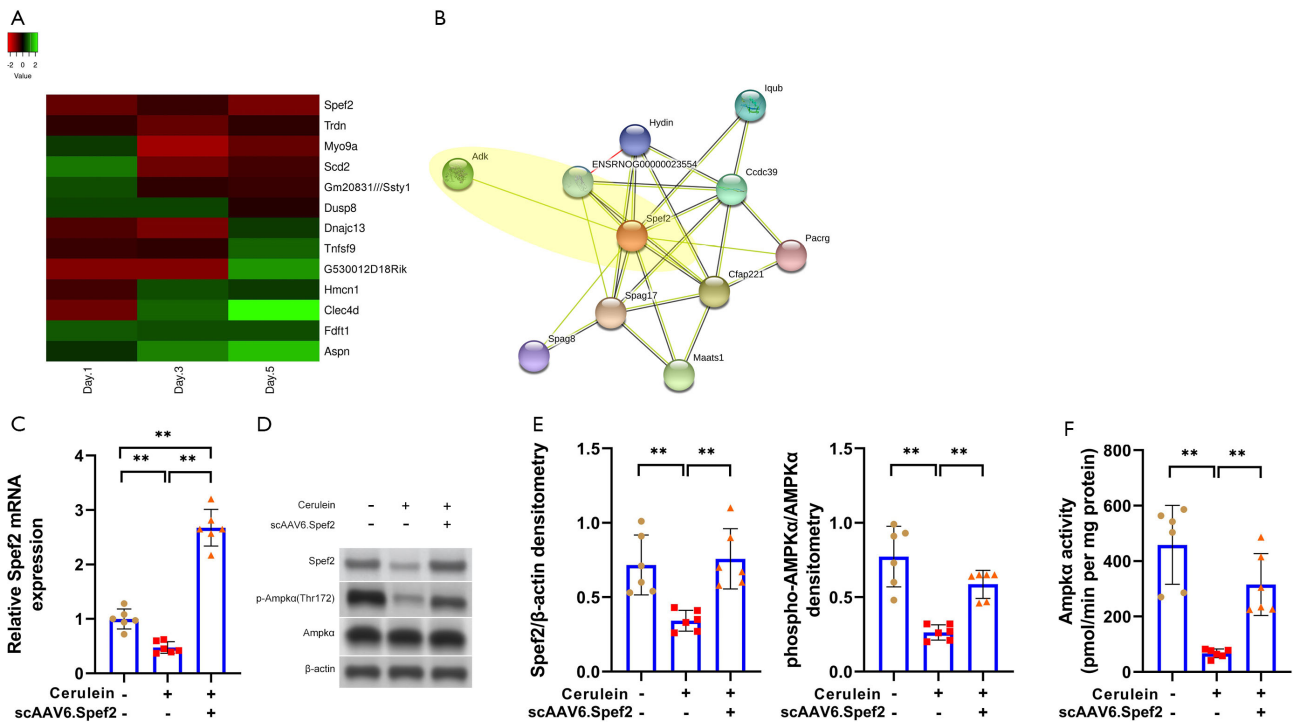

Figure S3 Spef2 overexpression promotes Ampkα phosphorylation and Ampkα activity in AR42J cells. (A) Heatmap of significantly dysregulated genes in microarray data derived from a murine model of cerulein-induced acute pancreatitis. (B) STRING protein-protein interaction analysis (medium confidence>0.040) reveals that rat Spef2 interacts with rat adenosine kinase (Adk). (C) qPCR of Spef2 mRNA expression in AR42J cells following adenoviral vector delivery of rat Spef2 (scAAV6.Spef2) or negative control (scAAV6.Ctrl). (D,E) Representative immunoblots and ImageJ densitometric quantitation of Spef2 expression and Ampkα^{Thr172} phosphorylation and (F) Ampkα activity assay in scAAV6.Ctrl AR42J cells and scAAV6.Spef2 AR42J cells. Data represented as means ± SDs. N=3 biological replicates ×2 technical replicates. **P<0.01 (one-way ANOVA with Bonferroni post-hoc).

© Annals of Translational Medicine. All rights reserved.
https://dx.doi.org/10.21037/atm-22-3118

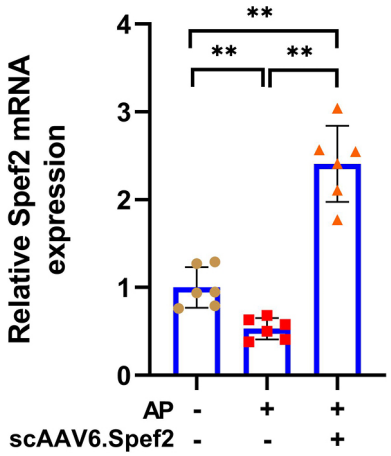

Figure S4 qPCR validation of Spef2 overexpression in scAAV6.Spef2 rats. Quantitation of pancreatic tissue *Spef2* mRNA expression by qPCR. *Gapdh* used as housekeeping control. Data represented as means ± SDs. N=6 rats per cohort. **P<0.01 (one-way ANOVA with Bonferroni post-hoc).

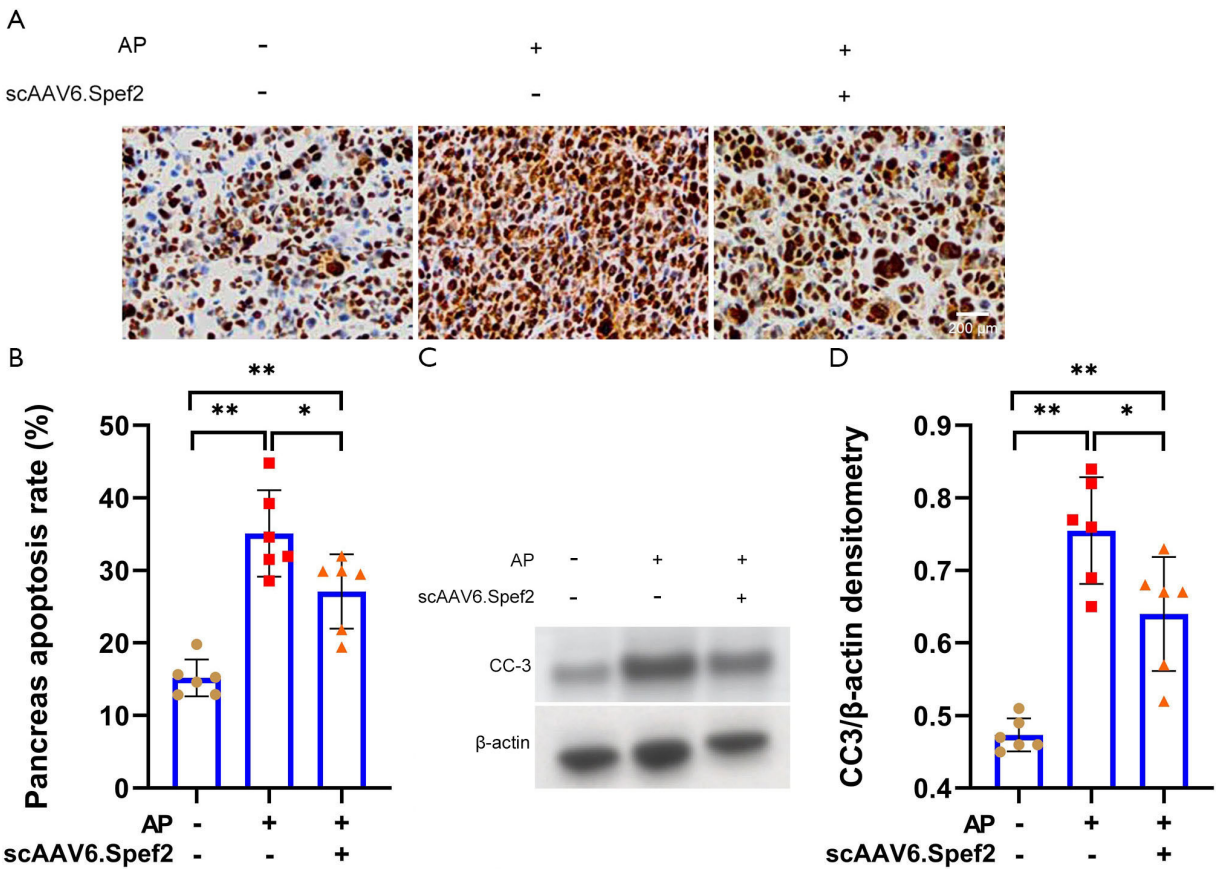

Figure S5 Spef2 overexpression during acute pancreatitis reduces cell apoptosis. (A) Representative TUNEL staining measuring (B) pancreatic cell apoptosis in tissues from the treatment groups described in Figure 2. (C,D) Representative immunoblots and ImageJ densitometric quantitation of pancreatic cleaved caspase-3 (CC-3) expression. Data represented as means ± SDs. N=6 rats per cohort. *P<0.05, **P<0.01 (one-way ANOVA with Bonferroni post-hoc).

© Annals of Translational Medicine. All rights reserved.
https://dx.doi.org/10.21037/atm-22-3118

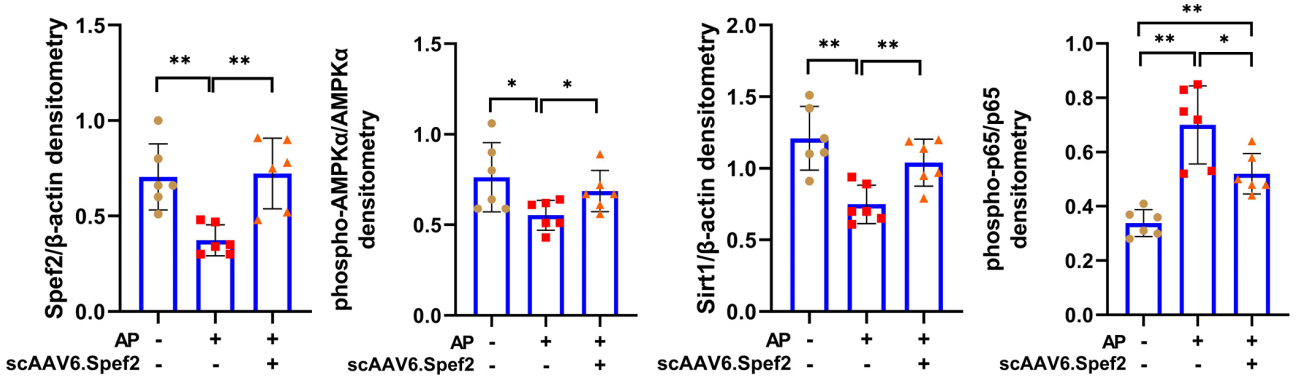

Figure S6 Densitometric analysis of Figure 2F immunoblots. Quantitation of pancreatic Spef2 and Ampkα/Sirt1/NF-κB signalling protein expression by ImageJ densitometry. β-actin used as loading control. Data represented as means ± SDs. N=6 rats per cohort. *P<0.05, **P<0.01 (one-way ANOVA with Bonferroni post-hoc).

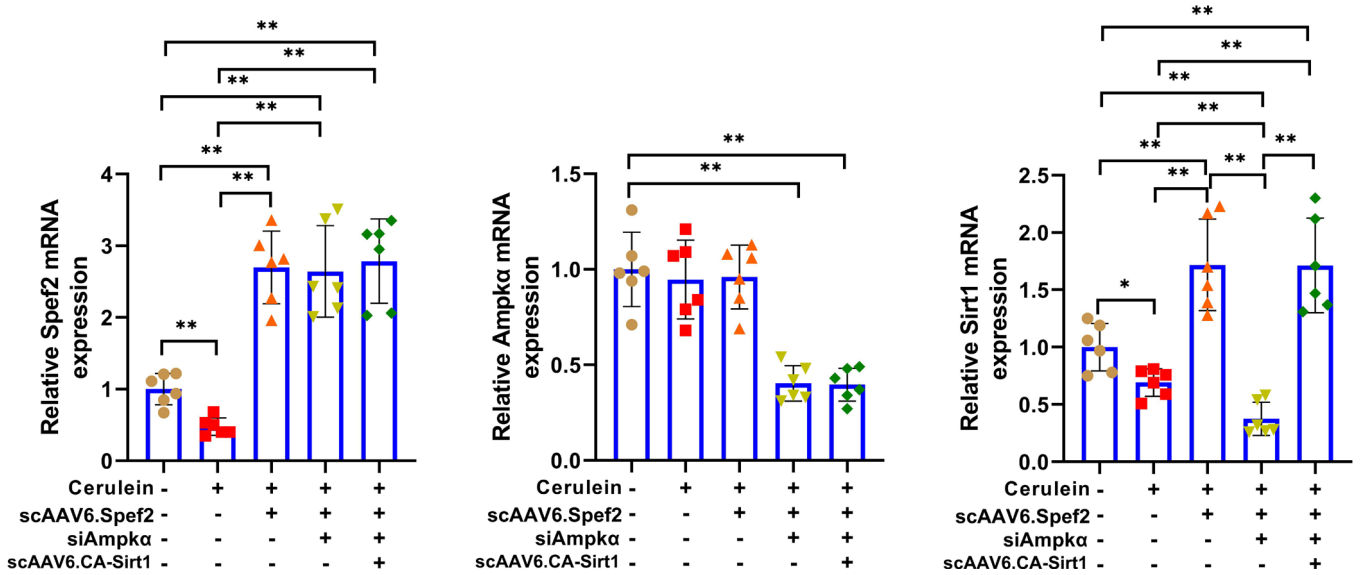

Figure S7 qPCR validation of gene overexpression and silencing in AR42J cells. Quantitation of AR42J cell *Spef2*, *Ampkα*, and *Sirt1* mRNA expression by qPCR. *Gapdh* used as housekeeping control. Data represented as means ± SDs. N=3 biological replicates ×2 technical replicates. *P<0.05, **P<0.01 (one-way ANOVA with Bonferroni post-hoc).

© Annals of Translational Medicine. All rights reserved.
https://dx.doi.org/10.21037/atm-22-3118

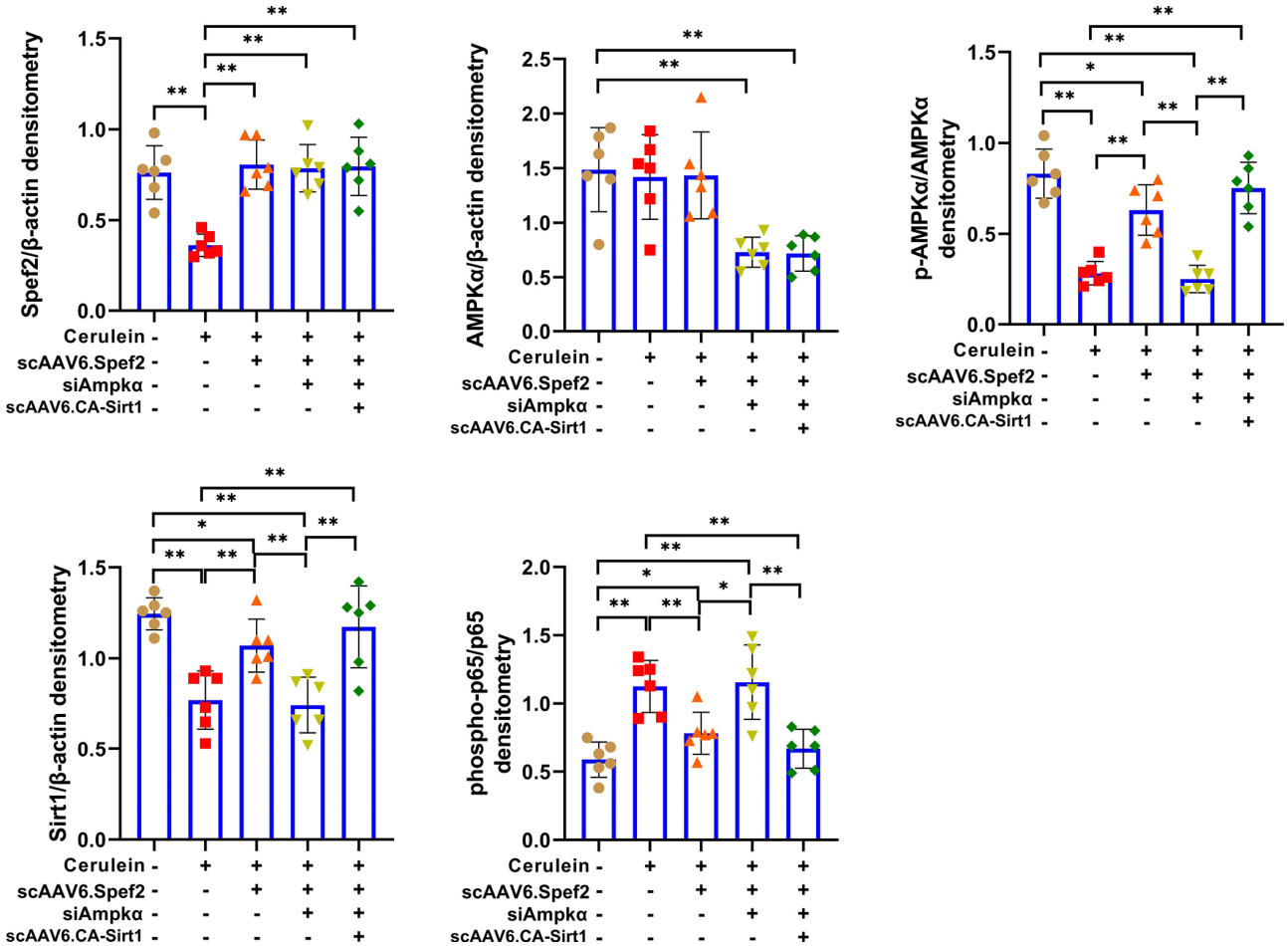

Figure S8 Densitometric analysis of Figure 3A immunoblots. Quantitation of AR42J cell Spef2 and Ampkα/Sirt1/NF-κB signalling protein expression by ImageJ densitometry. β-actin used as loading control. Data represented as means ± SDs. N=3 biological replicates × 2 technical replicates. *P<0.05, **P<0.01 (one-way ANOVA with Bonferroni post-hoc).

© Annals of Translational Medicine. All rights reserved.
https://dx.doi.org/10.21037/atm-22-3118

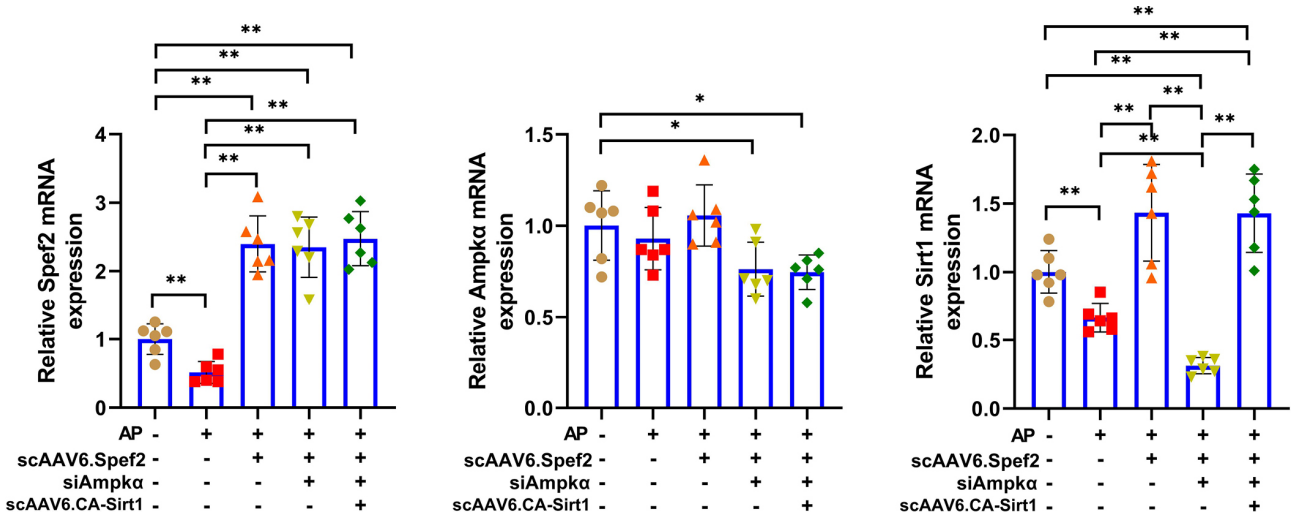

Figure S9 qPCR validation of gene overexpression and silencing in model rats. Quantitation of pancreatic tissue *Spef2*, *Ampkα*, and *Sirt1* mRNA expression by qPCR. *Gapdh* used as housekeeping control. Data represented as means ± SDs. N=6 rats per cohort. *P<0.05, **P<0.01 (one-way ANOVA with Bonferroni post-hoc).

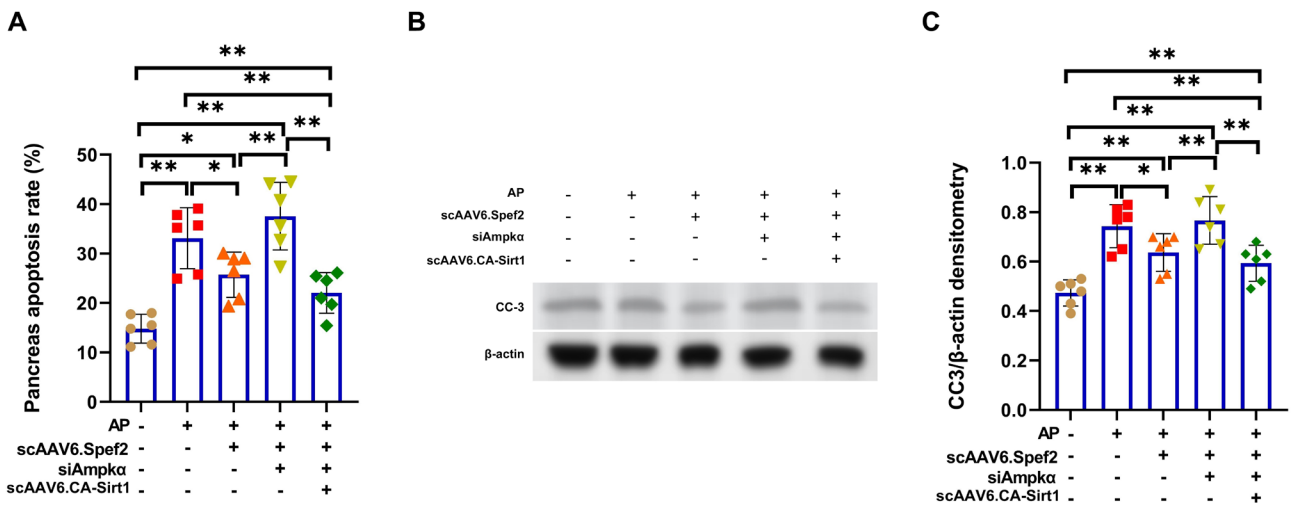

Figure S10 Spef2 overexpression during acute pancreatitis reduces cell apoptosis in a Sirt1/Ampk-dependent manner. (A) TUNEL staining-based assessment of pancreatic cell apoptosis in tissues from the treatment groups described in Figure 4. (B,C) Representative immunoblots and ImageJ densitometric quantitation of pancreatic cleaved caspase-3 (CC-3) expression. Data represented as means ± SDs. N=6 rats per cohort. *P<0.05, **P<0.01 (one-way ANOVA with Bonferroni post-hoc).

© Annals of Translational Medicine. All rights reserved.
https://dx.doi.org/10.21037/atm-22-3118

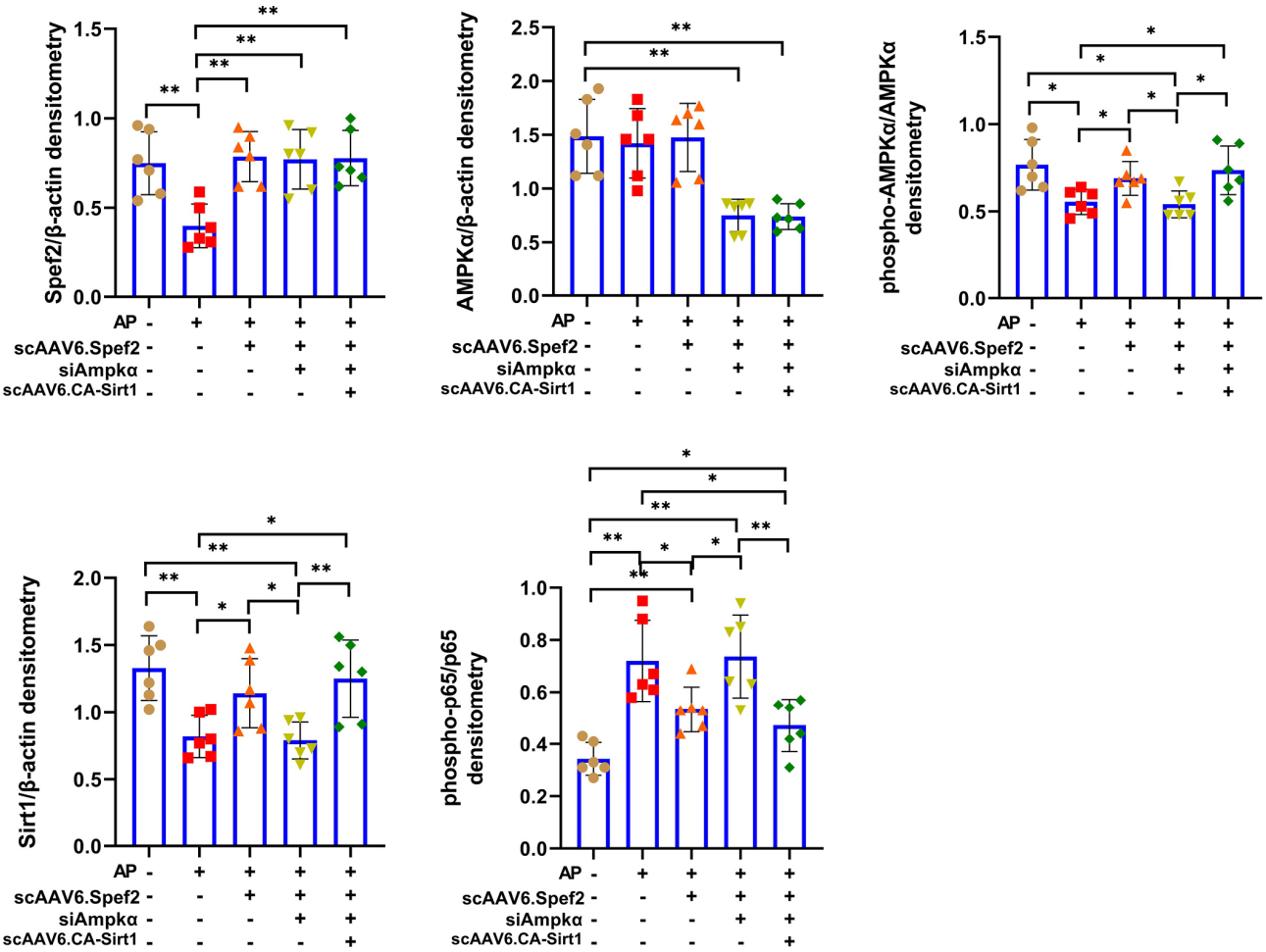

Figure S11 Densitometric analysis of Figure 4F immunoblots. Quantitation of pancreatic Spef2 and Ampkα/Sirt1/NF-κB signalling protein expression by ImageJ densitometry. β-actin used as loading control. Data represented as means ± SDs. N=6 rats per cohort. *P<0.05, **P<0.01 (one-way ANOVA with Bonferroni post-hoc).

© Annals of Translational Medicine. All rights reserved.
https://dx.doi.org/10.21037/atm-22-3118